Effects of chemical species and nonlinear thermal radiation on 3D Maxwell nanofluid flow with double stratification

Thesis Submitted By:

SANIA NASEER (01-248172-009)

Supervised By:

Prof. Dr. M. Ramzan

A dissertation submitted to the Department of Computer Science, Bahria University, Islamabad as a partial fulfillment of the requirements for the award of the degree of MS

Session(2017-2019)

Bahria University
Discovering Knowledge

MS-13

Thesis Completion Certificate

Student's Name: **Sania Naseer** Registration No. **01-248172-009**

Program of Study: **MS(Mathematics)**

Thesis Title: **"Effects of chemical species and non-linear thermal radiation on 3D Maxwell nonofluid flow with double stratification."**

It is to certify that the above student's thesis has been completed to my satisfaction and, to my belief, its standard is appropriate for submission for Evaluation. I have also conducted plagiarism test of this thesis using HEC prescribed software and found similarity index at **12%** that is within the permissible limit set by the HEC for the MS/MPhil degree thesis. I have also found the thesis in a format recognized by the BU for the MS/MPhil thesis.

Principal Supervisor's Signature: 21/06/2019

Date: 21-06-2019 **Name: Prof. Dr. M. Ramzan**

Bahria University
Discovering Knowledge

MS-14A

Author's Declaration

I, Sania Naseer hereby state that my MS thesis titled "Effects of chemical species and non-linear thermal radiation on 3D Maxwell nonofluid flow with double stratification"

is my own work and has not been submitted previously by me for taking any degree from this university

Bahria University Islamabad campus

or anywhere else in the country/world.

At any time if my statement is found to be incorrect even after my Graduate the university has the right to withdraw/cancel my MS degree.

Name of student: Sania Naseer

Date: 21-06-2019

Bahria University
Discovering Knowledge

MS-14B

Plagiarism Undertaking

I, solemnly declare that research work presented in the thesis titled "**Effects of chemical species and nonlinear thermal radiation on 3D Maxwell nanofluid flow with double stratification**"

is solely my research work with no significant contribution from any other person small contribution / help wherever taken has been duly acknowledged and that complete thesis has been written by me.

I understand the zero tolerance policy of the HEC and Bahria University towards plagiarism. Therefore I as an Author of the above titled thesis declare that no portion of my thesis has been plagiarized and any material used as reference is properly referred / cited.

I undertake that if I am found guilty of any formal plagiarism in the above titled thesis even after award of MS degree, the university reserves the right to withdraw / revoke my MS degree and that HEC and the University has the right to publish my name on the HEC / University website on which names of students are placed who submitted plagiarized thesis.

Student / Author's Sign: 

Name of the Student: **Sania Naseer**

Dedicated to
My beloved mother and respected supervisor

Acknowledgments

Words are bound and knowledge is limited to praise **ALLAH** the beneficent, the merciful who universe and bestowed mankind with the knowledge and ability to think into his secrets. Then the trembling lips and wet eyes praise the greatest man of universe, the last messenger of **ALLAH, HAZRAT MUHAMMAD (PBUH)**, whom **ALLAH** has sent as mercy for worlds, the illuminating torch, the blessing for the literate, illiterate, rich, poor, powerful, weaker, and able and disable.

My acknowledgment is to my kind, diligent and highly zealous supervisor, Prof. Dr. M. Ramzan, who supported me with his cherished opinions and inspirational discussions. His valuable expertise, comments, suggestions and instructions are most welcome that greatly improved the clarity of this document.

My gratitude is to my honorable professors who took me to the apex of my academia with their guidance. In particular, Dr. Rizwan-ul-haq and Dr. Jafar Hasnain who have always been supportive in all of my course work and kept encouraging me throughout the session in Bahria University, Islamabad Campus. They are the true teachers who have made Mathematics Department of BUIC, a real place of learning.

My intense recognition is to my mother, brothers and sister, who are always real pillars for my encouragement and showered their everlasting love, care and support throughout my life. I am very grateful to Hina Gul who support and guided me at every stage, my friends Nazia Shahmir, Asma Touqeer and Hina Satti were specially remained enormously helpful throughout the period of my MS studies.

Sania Naseer

Bahria University Islamabad, Pakistan

May 2019

Abstract

This mathematical analysis refined, magnetohydrodynamic (MHD) 3D flow of Maxwell nanoliquid in the existence of heat generation/absorption. Effects of nonlinear thermal radiation and chemical reaction are also added. Flow analysis is performed in the presence of thermal and concentration stratification boundary conditions. Boundary layer system of nonlinear partial differential equations (PDEs) are converted into ordinary differential equations with high nonlinearity. Homotopy Analysis method (HAM) is employed to regulate the mathematical analysis. The obtained results for velocity, temperature and concentration profiles are analyzed graphically for various admissible parameters. The impact of the Nusselt number for distinct parameters is also discussed and explored. The results obtained in the analysis are substantiated by erecting a comparative table with an established result in the literature. An outstanding matching is achieved in this regard.

LIST OF TABLES

LIST OF FIGURES

NOMENCLATURE

x, y, z	Coordinate axis
u, v, w	Velocity components
B_0	Magnetic field strength
μ	Dynamic viscosity
λ_1	Relaxation time
λ_2	Retardation time
ρ_f	Density of base fluid
ν	Kinematic viscosity
$(\rho c)_f$	Heat capacity of fluid
Q	Heat generation/absorption coefficient
T	Temperature
T_∞	Temperature far away from the surface
α	Thermal diffusivity of fluid
K	Thermal conductivity
c_p	Specific heat capacity
q_r	Radiative heat flux
q_w	Wall heat flux
C	Nano particles concentration
C_∞	Concentration far away from the surface
k^*	Coefficient of mean absorption

Re_x	Local Reynolds number
k_r	Reaction rate constant
C_0	Reference concentration
T_f	Fluid temperature
C_f	Convective fluid concentration
σ^*	Stefan-Boltzman constant
D_T	Thermophoretic diffusion coefficient
k	Chemical reaction parameter
M	Magnetic parameter
β_1	Deborah number in expression of relaxation time
θ_w	Temperature ratio parameter
$(\rho c)_p$	Effective heat capacity of nanoparticles
D_B	Brownian diffusivity coefficient
η	Similarity variable
θ	Dimensionless temperature
ϕ	Dimensionless concentration
f	Dimensionless velocity
Sc	Schmidt number
S	Heat generation/absorption parameter
T_0	Reference temperature
Pr	Prandtl number

Nb	Brownian motion parameter
Nt	Thermophoresis parameter
Rd	Radiation parameter
Nu_x	Nusselt number
S_1	Thermal stratification parameter
S_2	Concentration stratification parameter
β_2	Deborah number in expression of retardation time
γ	Biot number
τ_{yx}	Shear force
$\frac{du}{dy}$	Velocity gradient
Q_1	Heat transfer rate
L	Characteristic length
A	Cross sectional area
ΔT	Temperature difference
m	Mass of substance
V^*	Volume
P	Pressure
F	Force
n	Flow behavior index
k_1	Consistency index
h_f	Heat transfer coefficient

x_i	Coordinate at the boundary
T_w	Wall temperature
S^*	Extra stress tensor
$\frac{D}{Dt}$	Covariant differentiation
A_1	First Rivlin-Erickson tensor
$\frac{d}{dt}$	Material time derivative
τ	Cauchy stress tensor
De	Deborah number
t_{obs}	Time of observation
t	Matrix transpose
L^*	Strain tensor
λ	Ratio parameter
σ	Electrical conductivity
I	Identity matrix
a, b	Positive constants
l	Unit thickness of a substance

Contents

Chapter 1

Introduction and Literature review

1.1 Introduction

The flows of non-Newtonian liquids have significant role in several industrial and engineering processes, for example, paper production, petroleum drilling, plastic sheet formation, glass blowing, the expulsion of polymeric liquids and melts, biological solutions, asphalts, paints and so forth. Non-Newtonian liquids are defined as materials which do not show the direct or linear correspondence between shear stress and velocity gradient. For this class of liquids, an infinite number of possible rheological relationships exist. Rheological characteristics of non-Newtonian liquids differ a lot than the Newtonian liquids. No doubt, the rheological properties of all the non-Newtonian liquids cannot be predicted by one constitutive equation between shear rate and rate of strain. As for non-Newtonian liquids, there is always a nonlinear relationship between the stress and the rate of strain. The constitutive equations in non-Newtonian liquids are much complicated, more nonlinear and higher order in comparison to the Newtonian liquids. These liquids may be conveniently grouped into three general classes:

- Fluids for which the rate of shear at any point is determined only by the value of the shear stress at that point at that instant; these liquids are variously known as "time independent", "inelastic", "purely viscous" or "generlized Newtonian liquids".

- More complex liquids for which the relation between shear stress and shear rate depends, in addition, upon the duration of shearing and their kinematic history; they are called

"time dependent liquids"

- Substances exhibiting characteristics of both ideal fluids and elastic solids and showing partial elastic recovery and after deformation these are categorizesd as "visco-elastic liquids".

This classification scheme is arbitrary in that most real materials often exhibit a combination of two or even all three types of non-Newtonian features. This consideration is much too broad to be handled in the initial phases of the development. Therefore a particular rheological model will be selected for use initially, and application of the resulting development to fluids deviating from the assumed model will be considered subsequently. Several approximate and self-consistent non-Newtonian rheological models are proposed over the past decades as no single one can encompass assorted features of all the fluids. These models are classified into differential, rate and integral types. In particular, the stress relaxation in polymer processing is usually predicted using rate-type fluid models such as Maxwell, Oldroyd-B or Burgers fluids. Among these models, Maxwell liquid is a least complex subclass of rate type non-Newtonian liquids. This model is broadly used to investigate the impacts of stress relaxation. The inclusion of stress relaxation in the stress tensor of Maxwell liquid makes it highly nonlinear and completed in contrast with Newtonian liquid. Maxwell liquid model converted into the simple Navier Stokes equation when additional stress time is zero.

A nanofluid is a fluid containing nanometer sized particles, called nanoparticles. The nanoparticles used in nanofluids are typically made of metals, oxides, or carbon nanotubes. Common base fluids include water, ethylene glycol and oil. This fluid is different from other ordinary base fluids because they are prepared by dispersing nanoparticles in the base fluids. These particles are inserted into base fluids to improve the thermal conductivity and heat transfer performance. Nanoliquid is the ideal applicant to get position of working fluid. Having thermal conductivity more than the base fluid and a size of 1 - 100 nm, these substances are utilized to get the greatest improvement in the thermal characteristics under lower concentrations. Nanoliquids have the potential to significantly enhance heat transfer rates in a variety of zones such as nuclear reactors, industrial cooling applications, transportation industry, heat exchangers, micro-electromechanical systems, fiber and granular insulation, chemical

catalytic reactors, packed blood flow in the cardiovascular system engaging the Navier–Stokes equation. The improved thermal characteristics of naofluid has worth in numerous fields such as pharmaceutical processes, transportation, microelectronics, micromanufacturing, power generation, thermal therapy for cancer surgery air-conditioning, metallurgical and chemical sectors etc. In vehicles, the demand of nanofluids as coolants takes into consideration for good size and consequently this consumes smaller energy for controlling the road resistance. Owing to consequential improvements in automotive aerodynamics, there is large interest in breaking systems with more precise heat dissipation and stuff including brake nanofluid. Many researchers are recently interested to develop more efficient solar collectors with high absorpation of solar radiations.

The role of stratification is central in many natural and engineering processes. Stratification of liquid is a testimony or development of layers that happens because of temperature distributions, change in concentration or because of the existence of various liquids. The examination of thermal and solutal stratification of oxygen and hydrogen in lakes is essential in light of the fact that the development rate of every single refined species legitimately influenced by them. Thermal stratification appears due to temperature imbalance, which gives rise to a density imbalance in the fluid medium. Usually, the causes are thermal energy from heated bodies (e.g, sun). When sunlight falls on the surface of the lake it imposes the temperature change. This temperature change depends on the degree and depth of lake which is able to affect by wind and any source of heated bodies. When lake is stratified, three layers are formed within the lake, the upper warm layer referred to as epilimnion, and the deeper cold layer referred to as hypolimnion. The boundary layer between the two layers where the temperature change more rapidly referred to as thermocline. It is also observed that temperature imbalance may alter from layer to layer and these flows have wider applications in agriculture and oceanography. The concentration stratification is applicable in many phenomena like transportation in the sea, where stratification remains due to salinity imbalance. Due to the presence of different fluids, a stable stand point arises when the lighter fluid stands over the denser one.

Magnetohydrodynamics (MHD) is the science of motion of electrically conducting fluid in the presence of magnetic field. The study of MHD flow of an electrically conducting fluid is of considerable importance in an metallurgical and metal-working processes. This type of flow

problem has attracted the attention of numerous researchers due to its outstanding applications in many engineering problems such as MHD generators, nuclear reactors, plasma studies and geothermal energy extraction. Also hydromagnetic techniques are used for the purification of molten metals from non-metallic inclusions.

1.2 Literature review

Viscoelastic fluids have accomplished exclusive enthusiasm by current researchers in perspective of more extensive mechanical and engineering applications.The investigations on these fluids are remarkably enhanced during the past few decades because of their practical implications in technology and industrial processes. Many of the materials in our daily life include apple sauce, sugar solution, muds, chyme, soaps, emulsion, shampoos, blood at low shear rate etc. exhibits the characteristics of viscoelastic fluids. The analysis of non-Newtonian materials has engrossed continuous consideration of recent investigators. This fact of non-Newtonian materials is different from viscous materials. In the literature, there is no single relation that characterizes all the properties of non-Newtonian fluids. Thus various models of non-Newtonian fluids have been suggested. Among these models, Maxwell fluid is a simplest subclass of rate type non-Newtonian fluids. In view of such importance of Maxwell nanofluid, Ramzan et. al [1] explored the mixed convective flow of Maxwell nanofluid past a porous vertical stretched surface. Impact of double stratification and magnetic field in mixed convective radiative flow of Maxwell nanofluid is considered by Hussain et al. [2]. Bai et al. [3] presented towards a stretching sheet MHD stagnation flow of Maxwell nanofluid with thermophoresis and Brownian motion. Influence of homogeneous-heterogeneous reactions on MHD 3D Maxwell fluid flow with Cattaneo-Christov heat flux and convective boundary condition is analyzed by Ramzan et al. [4]. Jusoh et al. [5] discussed three dimensional flow of MHD Maxwell nanoliquids by a convectively heated permeable stretching sheet. Nonlinear thermal radiation flow of Maxwell nanofluid subjected to convectively heated stretched surface is detailed by Hayat et al. [6].

With the rapid progress of modern engineering technology, the nano-materials as a kind of new materials has got extensive attention due to its various applications in industrial, transportation, electronics and biomedicine. Recent advancements made it conceivable to diffuse

nanoparticles in ordinary heat transfer liquids including engine oil, ethylene glycol and water to create another class of heat transfer liquids with great effectiveness. Transfer of heat properties of Cu-water nanoliquid flow amid the parallel sheets are discussed by Sheikholeslami et al.[7]. MHD flow and temperature dependent viscosity of viscoelastic nanoliquid in a channel is presented by Ellahi [8]. Three-dimensional flow of an elastico-viscous nanofluid with chemical reaction and magnetic field effects considered by Ramzan et al. [9]. Different investigations have been directed to reveal the various aspects of the nanofluid in [10-17].

Stratification occurs due to the variations in temperature and concentration or present of different fluids of different densities. Simultaneous occurrence of heat and mass transfer is prime reason to trigger stratification. Many daily life occurrences like ground water reservoirs, manufacturing processes, estuaries, industrial foods and salinitystratification in rivers encounter stratification. In reservoirs, stratification minimize the mixing of oxygen to base water. In lakes and ponds, stratification maintains a balance in the ratio of hydrogen and oxygen by controlling the temperature and concentration differences to keep the enviroment suitable for species growth. Researchers and scientists are showing interest in explorations highlighting stratification phenomenon. In perspective of such importance of thermal/solutal stratification, Ibrahim et al. [18] investigated the viscous nanoliquid flow past a vertical plate in the existence of thermal and solutal stratifications. Here presented the numerical solutions of velocity, temperature and nanoparticles concentration. In mixed convection flow of Maxwell liquid, the influence of thermal stratification with thermal radiation is examined by Hayat et al. [19]. Flow of MHD free convection micropolar fluid past a vertical plate with double stratification is explored by Srinivasacharya et al. [20]. Simultaneous illustration of thermal radiation and thermal stratification in flow of jeffrey fluid over a stretching sheet is reported by Hayat et al. [21]. Some extraordinary observations about the research thermal and solute stratification under different perspectives can be found at [22-30] many therein.

Chemical reaction can be explained as an interaction between two or more chemicals which produces either one or more new chemical compounds. Many chemical reactions actually requires heat and accelerator (*i.e.* catalyst). A chemical reaction in which catalyst is in the same phase (*i.e.* in the same state of matter) as the reactant(s) is/are known as homogeneous catalytic reaction. Reactions between two gases, between two liquids and mixture of household

cooking gas with oxygen gas leading to flame are typical examples of homogeneous catalytic reactions. In heterogeneous catalytic reaction, catalyst and reactants are in different phases (*i.e.* different states of matter). Examples of heterogeneous catalytic reactions are chemical reactions between a gas and a liquid, a gas and a solid, and liquid and a solid. Analysis of activation energy in Couette-Poiseuille flow of nanofluid in the presence of chemical reaction and convective boundary conditions is studied by Zeeshan el at. [31]. Animasaun [32-34] reported chemically reacting fluid flow through binary mixture in micropolar fluid flow, nth order of chemical reaction in Casson fluid flow and quartic autocatalytic chemical reaction in47 nm alumina-water nanofluid within boundary layer. In prespective of its clarity, the remarkable work of current researchers, see few studies [35-40].

Chapter 2

Basic preliminaries and laws

This chapter contains some elementary definitions, concepts and laws that are helpful in understanding work in the subsequent chapters.

2.1 Fluid

A substance that consist of particles those constantly distorts when shear stress is applied. Oil, paints, blood, ketchup and water are some examples of fluid.

2.1.1 Liquid

It is type of fluid that has a definite volume but no definite shape. For example blood, water and milk etc.

2.1.2 Gas

Fluid that has no definite volume and shape is known as gas. Oxygen, hydrogen and nitrogen are examples of gases.

2.2 Fluid mechanics

The branch of mechanics that deals with the study of fluid's behavior at rest or in motion. It can be divided into two branches as follows:

2.2.1 Fluid statics

Fluid statics is the subclass of Fluid mechanics which deals with the fluid properties at rest.

2.2.2 Fluid dynamics

Fluid dynamics is the subclass of Fluid mechanics which deals with the fluid properties at motion.

2.3 Stress

Stress is defined as the force per unit area within the deformable body. The SI unit of stress is Nm^{-2} or $kg/m.s^2$ and dimension $\left[\frac{M}{LT^2}\right]$. Mathematically,

$$\tau_{ji} = \frac{F_i}{A_j} \qquad i, j = x, y, z, \tag{2.1}$$

where F_i, A_j are the componants of force and area respectively.

2.4 Types of stress

Stress is further divided into two types:

2.4.1 Shear stress

The force that acts on a material parallel to the unit area of the surface is categorized as shear stress.

2.4.2 Normal stress

The force that acts on a material perpendicular to the unit area of the surface is categorized as normal stress.

2.5 Flow

Flow is characterized as a material that distort easily and continuously under the impacts of various kind of forces.

2.6 Types of flow

There are two different ways to describe the flow:

2.6.1 Laminar flow

A flow in which every fluid substance has different layers of fluid and the layer of individual substances do not cross one another.

2.6.2 Turbulent flow

A flow in which every fluid substance has different layers of fluid and the layer of individual substances cross one another.

2.7 Viscosity

Viscosity is an intrinsic fluid property which describes the behavior and motion of the fluid nearest the boundary. By applying the shear stress the deformation occurs in fluid, then an internal quantity generates that measures the fluid flow resistance is called viscosity. *i.e,*

$$\mu = \tau_{yx} / \frac{du}{dy}. \tag{2.2}$$

There are two ways to describe the viscosity.

2.7.1 Dynamic viscosity

It is the fluid property that specifies the resistance of fluid against any deformation with the applied force. Mathematically, it can be expressed as

$$\text{viscosity } (\mu) = \frac{\text{shear stress}}{\text{gradient of velocity}}. \tag{2.3}$$

Its SI unit is Ns/m^2 and its dimension is $\left[\frac{M}{LT}\right]$.

2.7.2 Kinematic viscosity

It is the fluid property that specify the dynamic viscosity (μ) over the density of fluid (ρ). Mathematically, it is represented by

$$\text{Kinematic viscosity} = \nu = \frac{\mu}{\rho}. \tag{2.4}$$

Its SI unit is m^2/s and its dimension is $\left[\frac{L^2}{T}\right]$.

2.8 Newton's law of viscosity

The liquids which show the direct and linear relation between shear stress and velocity gradient. Mathematically, it can be expressed by

$$\tau_{yx} \propto \frac{du}{dy}, \tag{2.5}$$

or

$$\tau_{yx} = \mu \left(\frac{du}{dy}\right), \tag{2.6}$$

where τ_{yx} denotes the shear force, μ the proportionality constant and $\frac{du}{dy}$ the velocity gradient.

2.9 Viscous Fluids

A fluid characterizes as viscous fluid if its viscosity may change or uniform due to different type of stresses. These fluids can be subdivided as follows:

2.9.1 Newtonian fluids

Newtonian fluids are those liquids which follow the Newton's law of viscosity or show the direct and linear correspondence between shear stress and velocity gradient. In these liquids shear force (τ_{yx}) is linearly proportional to the gradient of velocity $\left(\frac{du}{dy}\right)$ and μ is constant here. Air, water and glycerin are common examples of Newtonian fluids.

2.10 Non-Newtonian fluids

Non-newtonian fluids are those liquids which do not follow the Newton's law of viscosity or do not show the direct and linear correspondence between shear stress and velocity gradient. Here, nonlinear and direct relationship exists between shear stress ($\boldsymbol{\tau}_{yx}$) and gradient of velocity $\left(\frac{du}{dy}\right)$. Mathematically, it is stated as

$$\boldsymbol{\tau}_{yx} \propto \left(\frac{du}{dy}\right)^{n}, \ n \neq 1, \tag{2.7}$$

or

$$\boldsymbol{\tau}_{yx} = \eta_1 \frac{du}{dy}, \ \eta_1 = k_1 \left(\frac{du}{dy}\right)^{n-1}, \tag{2.8}$$

where η_1, n and k_1 represents apparent viscosity, flow behavior index and consistency index respectively. For $n = 1$ Eq. (2.8) shows the expression for Newton's law of viscosity.

Examples of Non-Newtonian fluids are honey, ketchup, paints, blood, tooth paste and polymer solutions etc. These liquids are divided into three major types *i.e,* (i) differential type (ii) integral type and (iii) rate type. The Maxwell fluid model under discussion in this dissertation is subdivided into rate type fluids.

2.10.1 Rate type fluids

Rate type fluids are those which exhibits the behaviour of relaxation and retardation times phenomena. In rate type fluids stress is given implicitly in terms of velocity gradient and its higher derivatives. Examples of rate type fluid models are Maxwell, Oldroyd, Burgers and Jeffery fluids etc.

2.10.2 Retardation Time

The time needed to balance an opposing force which is generated when shear stress acts.

2.10.3 Relaxation Time

The system transform from equilibrium position to perturb position with the applied stress, When the system is free of stress the time needed for a perturb system back to equilibrium position is known as relaxation time.

2.11 Density

Density is defined as mass of a substance per unit volume or ratio between mass and volume. This quantity is utilized to quantify that how much material of a substance present in unit volume.

Mathematically,

$$\rho = \frac{m}{V^*}, \tag{2.9}$$

where m denotes the mass of the substance and V^* is the volume. The SI unit of density is kg/m^3.

2.12 Pressure

It is define as a magnitude of force that applied perpendicular to the surface per unit area. Mathematical expression for the pressure is given as

$$P = \frac{F}{A}. \tag{2.10}$$

The SI unit of pressure is N/m^2.

2.13 Thermal diffusivity

Thermal diffusivity is a material specific property for explaining the unsteady conductive heat flow. This value describes how speedily a material respond to change in temperature. It is proportion of the thermal conductivity to the product of specific heat capacity and density. Mathematically,

$$\alpha = \frac{K}{\rho\,(c_p)}, \tag{2.11}$$

where K denotes the thermal conductivity, c_p the specific heat capacity and ρ the density.

2.14 Thermal conductivity

Thermal conductivity is a substance specific property that identify the heat conduction. This value illustrates that how much heat is conveyed to the materials. From the Fourier's law for heat conduction, it is expressed as a ratio of heat transfered (Q_1) with unit thickness of a substance (l) per unit time and per unit surface area (A) over the temperature difference (ΔT).

Mathematically,

$$K = \frac{Q_1 l}{A(\Delta T)}.$$

In SI unit it is measured in kgm/s^3K and its dimension is $(\frac{ML}{T^3\theta})$.

2.15 Convective boundary conditions

Convective boundary conditions are some time called Robin boundary conditions. These type of conditions are mostly describe on wall. Mathematically, these are communicated as:

$$K\left(\frac{\partial T}{\partial m_i}\right)_{x_i} = h_f\left(T_f(x_i,t) - T_w(x_i,t)\right), \tag{2.12}$$

where h_f indicates the heat transfer coefficient , x_i is the coordinate at the boundary, T_f is the convective fluid temperature and T_w is the wall temperature.

2.16 Stratification

Sometimes the phenomenon of changing density appeared in the shallow fluid medium owing to change in the state of concentration, pressure, temperature and dissolved substances known as stratification. It is highly observed that in the case of stratification, density is the function of space variable as well as time. Due to which layer formulation occurs. Following are the two subclasses of stratification.

2.16.1 Thermal stratification

Thermal stratification appears due to temperature imbalance, which gives rise to a density imbalance in the fluid medium. Usually, the causes are thermal energy from heated bodies (*e.g,*

sun). When sunlight falls on the surface of the lake it imposes the temperature change. This temperature change depends on the degree and depth of lake which is able to affect by wind and any source of heated bodies. When lake is stratified, three layers are formed within the lake, the upper warm layer referred to as epilimnion, and the deeper cold layer refferred to as hypolimnion. The boundary layer between the two layers where the temperature change more rapidly referred to as thermocline. It is also observed that temperature imbalance may alter from layer to layer and these flows have wider applications in agriculture and oceanography.

2.16.2 Concentration stratification

The concentration stratification is applicable in many phenomena like transportation in the sea, where stratification remains due to salinity imbalance. Due to the presence of different fluids, a stable standpoint arises when the lighter fluid stands over the denser one.

2.17 Maxwell fluid model

Extra stress tensor S^* for Maxwell liquid is

$$\left(1+\lambda_1\frac{D}{Dt}\right)S^* = S^* + \lambda_1\frac{DS^*}{Dt} = \mu A_1, \tag{2.13}$$

where λ_1 stands for relaxation time, D/Dt for covariant differentiation, μ for dynamic viscosity and A_1 for first Rivlin-Erickson tensor. First Rivlin-Erickson tensor is

$$A_1 = (\operatorname{grad} v)^t + \operatorname{grad} v, \tag{2.14}$$

in which t exhibits matrix transpose. For three dimensional $(3D)$ flow, we get

$$A_1 = \begin{bmatrix} 2u_x & u_y+v_x & u_z+w_x \\ u_y+v_x & 2v_y & v_z+w_y \\ u_z+w_x & v_z+w_y & 2w_z \end{bmatrix} \tag{2.15}$$

For tensor S^* of rank two, vector b_1 and scalar φ, we have

$$\frac{DS^*}{Dt} = \frac{\partial S^*}{\partial t} + (v.\nabla)\, S^* - S^* \left(\operatorname{grad} v\right)^t - \left(\operatorname{grad}(v)\, S^*\right), \tag{2.16}$$

$$\frac{Db_1}{Dt} = \frac{\partial b_1}{\partial t} + (v.\nabla)\, b_1 - (\operatorname{grad} v)\, b_1, \tag{2.17}$$

$$\frac{D\varphi}{Dt} = \frac{\partial \varphi}{\partial t} + (v.\nabla)\, \varphi. \tag{2.18}$$

Applying the operator $\left(1 + \lambda_1 \frac{D}{Dt}\right)$ on law of momemtum conservation from Eq.(2.46) , we get the following expression in the absence of body forces

$$\rho \left(1 + \lambda_1 \frac{D}{Dt}\right) \frac{dv}{dt} = - \left(1 + \lambda_1 \frac{D}{Dt}\right) \nabla_p + \left(1 + \lambda_1 \frac{D}{Dt}\right) (\nabla.S^*). \tag{2.19}$$

By adopting the procedure

$$\frac{D}{Dt}(\nabla.) = \nabla. \left(\frac{D}{Dt}\right), \tag{2.20}$$

applying Eq. (2.20) in Eq. (2.19) , we obtain

$$\rho \left(1 + \lambda_1 \frac{D}{Dt}\right) \frac{dv}{dt} = - \left(1 + \lambda_1 \frac{D}{Dt}\right) \nabla_p + \nabla. \left(1 + \lambda_1 \frac{D}{Dt}\right) S^*, \tag{2.21}$$

using Eq. (2.13) in Eq. (2.21) , we get

$$\rho \left(1 + \lambda_1 \frac{D}{Dt}\right) \frac{dv}{dt} = - \left(1 + \lambda_1 \frac{D}{Dt}\right) \nabla_p + \mu (\nabla.A_1). \tag{2.22}$$

In the absence of pressure gradient, the above equation takes the form

$$\rho \left(1 + \lambda_1 \frac{D}{Dt}\right) \frac{dv}{dt} = \mu (\nabla.A_1). \tag{2.23}$$

Thus, above epression for steady Maxwell liquid flow is expressed by:

$$uu_x + vu_y + wu_z + \lambda_1 \begin{pmatrix} u^2 u_{xx} + v^2 u_{yy} + w^2 u_{zz} \\ +2uvu_{xy} + 2vwu_{yz} + 2uzu_{xz} \end{pmatrix} = \nu (u_{xx} + u_{yy} + u_{zz}), \tag{2.24}$$

$$uv_x + vv_y + wv_z + \lambda_1 \begin{pmatrix} u^2 v_{xx} + v^2 v_{yy} + w^2 v_{zz} \\ +2uvv_{xy} + 2vwv_{yz} + 2uwv_{xz} \end{pmatrix} = \nu \left(v_{xx} + v_{yy} + v_{zz} \right), \tag{2.25}$$

$$uw_x + vw_y + ww_z + \lambda_1 \begin{pmatrix} u^2 w_{xx} + v^2 w_{yy} + w^2 w_{zz} \\ +2uvw_{xy} + 2vww_{yz} + 2uww_{xz} \end{pmatrix} = \nu \left(w_{xx} + w_{yy} + w_{zz} \right). \tag{2.26}$$

2.18 Oldroyd-B fluid model

Extra stress tensor S^* for an Oldroyd-B liquid is expressed by

$$\left(1 + \lambda_1 \frac{D}{Dt}\right) S^* = S^* + \lambda_1 \frac{DS^*}{Dt} = \mu \left(1 + \lambda_2 \frac{D}{Dt}\right) A_1, \tag{2.27}$$

in which λ_2 exhibits retardation time and law of momemtum conservation in the absence of body force and pressure gradient can be written by

$$\rho \left(1 + \lambda_1 \frac{D}{Dt}\right) \frac{dv}{dt} = \mu \left(1 + \lambda_2 \frac{D}{Dt}\right) (\nabla . A_1). \tag{2.28}$$

The above equation in componant form gives

$$uu_x + vu_y + wu_z + \lambda_1 \begin{pmatrix} u^2 u_{xx} + v^2 u_{yy} + w^2 u_{zz} \\ +2uvu_{xy} + 2vwu_{yz} + 2uwu_{xz} \end{pmatrix}$$

$$= v \left(u_{zz} + \lambda_2 \begin{pmatrix} uu_{xzz} + vu_{yzz} + wu_{zzz} \\ -u_x u_{zz} - u_y v_{zz} - u_z w_{zz} \end{pmatrix} \right), \tag{2.29}$$

$$uv_x + vv_y + wv_z + \lambda_1 \begin{pmatrix} u^2 v_{xx} + v^2 v_{yy} + w^2 v_{zz} \\ +2uvv_{xy} + 2vwv_{yz} + 2uwv_{xz} \end{pmatrix}$$

$$= v \left(v_{zz} + \lambda_2 \begin{pmatrix} uv_{xzz} + vv_{yzz} + wv_{zzz} - \\ v_x u_{zz} - v_y v_{zz} - v_z w_{zz} \end{pmatrix} \right), \tag{2.30}$$

$$uw_x + vw_y + ww_z + \lambda_1 \begin{pmatrix} u^2 w_{xx} + v^2 w_{yy} + w^2 w_{zz} \\ +2uvw_{xy} + 2vww_{yz} + 2uwv_{xz} \end{pmatrix}$$

$$= v\left(w_{zz} + \lambda_2\left(\begin{array}{c} uw_{xzz} + vw_{yzz} + ww_{zzz} - \\ w_x u_{zz} - w_y v_{zz} - w_z w_{zz} \end{array}\right)\right). \tag{2.31}$$

2.19 Dimensionless numbers

2.19.1 Prandtl number

Momentum diffusivity (ν) to thermal diffusivity (α) ratio is termed as Prandtl number.

Mathematically, it has the following form

$$\mathrm{Pr} = \frac{\nu}{\alpha} = \frac{\mu c_p}{K}, \tag{2.32}$$

in which μ represents the dynamic viscosity, c_p denotes the specific heat and K stands for thermal conductivity. In heat transfer, Prandtl number is used to control the thicknesses of momentum and thermal boundary layers.

2.19.2 Schmidt number

It is the dimensionless number which describes the ratio between kinematic viscosity and mass diffusivity. Mathematically,

$$Sc = \frac{\nu}{D_B}, \tag{2.33}$$

where $\nu = \mu/\rho$ is the kinematic viscosity and D_B is the mass diffusivity.

2.19.3 Biot number

Biot number is a dimensionless quantity which finds connection between the resistance of internal substance to the resistance at the surface of the substance. Mathematically,

$$\text{Biot number} = \frac{\text{Resistance of internal substance}}{\text{Resistance of surface of substance}},$$

$$\gamma = \frac{h_f L}{K}, \tag{2.34}$$

where h_f is the heat transfer coefficient, L is the characteristic length and K is the thermal conductivity of the solid body.

2.19.4 Thermophoresis parameter

Thermophoresis is a mechanism which is used to prevent the mixing of different particles due to a pressure gradient when they move together or separate the mixture of particles after mixing up. In a cold surface thermophoresis is positive and it is negative for a hot surface.

Mathematically, it can be written as:

$$Nt = \frac{\tau D_T (T_f - T_0)}{\upsilon T_\infty}, \tag{2.35}$$

where T_f and T_∞ are the wall temperature and temperature outside the plate, T_0 is the reference temperature, D_T is thermophoretic diffusion coefficient, τ is the ratio of effective heat and heat capacity of the nanoparticles and υ the kinematic viscosity.

2.19.5 Brownian motion parameter

Brownian motion occurs due to size of the nanoparticles in a nanofluid. It is a nanoscale mechanism that displays the thermal influences of nanofluid. Mathematically,

$$Nb = \frac{\tau D_B (C_\infty)}{\upsilon}, \tag{2.36}$$

where

$$\tau = \frac{(\rho c)_p}{(\rho c)_f}. \tag{2.37}$$

In the above equation τ is the ratio of effective heat and heat capacity of the nanoparticles and fluid respectively, υ the kinematic viscosity, C_∞ the ambient concentration and and D_B the brownian diffusion coefficient.

2.19.6 Deborah number

A dimensionless number used to specify fluidity of materials. It is defined as the ratio of relaxation time to observation time. This specifies both elastic and viscous properties of materials.

The higher the Deborah number, the closer it is to a perfect solid. Mathematically,

$$D_e = \frac{\text{relaxation time}}{\text{time of observation}} = \frac{\lambda_1}{t_{obs}}. \tag{2.38}$$

2.19.7 Radiation parameter

The radiation parameter defines the relative contribution of conduction heat transfer to thermal radiation transfer, which can be expressed as follows:

$$Rd = \frac{4\sigma^* T_\infty^3}{Kk^*}, \tag{2.39}$$

here K the thermal conductivity, k^* is the absorption parameter, T_∞ for ambient temperature and σ^* indicates Stefan-Boltzman constant.

2.19.8 Chemical reaction parameter

The non-dimensional number used to measure the strength of chemical reaction rate is called chemical reaction parameter and can be written as:

$$k = \frac{k_r^2}{a}, \tag{2.40}$$

where k_r represents the reaction rate constant.

2.19.9 Nusselt number

The dimensionless number that represents the relationship between convection and conduction heat transfer coefficients at the bondary is known as Nusselt number. Mathematically,

$$Nu_L = \frac{h_f \triangle T}{K \triangle T/L} = \frac{h_f L}{K}, \tag{2.41}$$

where h_f, L and K represents convective heat transfer coefficient, characteristic length and thermal conductivity of fluid respectively.

2.20 Fundamental laws

The basic laws that are used for the flow description in the subsequential analysis are given below.

2.20.1 Law of mass conservation

Conservation law of mass states that the total mass in any system will remain same. Differential form of law of mass conservation is

$$\frac{\partial \rho}{\partial t} + (v.\boldsymbol{\nabla})\,\rho + \rho \boldsymbol{\nabla}.\mathbf{v} = 0, \tag{2.42}$$

or

$$\frac{\partial \rho}{\partial t} + \boldsymbol{\nabla}.\,(\rho \mathbf{v}) = 0, \tag{2.43}$$

in which ρ is fluid density, $\frac{d}{dt}$ is the material time derivative and v is the velocity of fluid. It is also known as the equation of continuity. For the steady flow Eq. (2.43) becomes

$$\boldsymbol{\nabla}.\,(\rho \mathbf{v}) = 0, \tag{2.44}$$

and if the fluid is incompressible then Eq. (2.44) implies that

$$\boldsymbol{\nabla}.\mathbf{v} = 0. \tag{2.45}$$

2.20.2 Law of momentum conservation

This law describes that the total linear momentum remains constant of a closed system. Differential form of law of momentum conservation is

$$\rho \frac{D\mathbf{v}}{Dt} = \operatorname{div} \boldsymbol{\tau} + \rho \mathbf{b}. \tag{2.46}$$

In Eq.(2.46) left hand side represents an internal force, 1^{st} term on right hand side for the surface force and 2^{nd} term the body force, where b stands for body force and $\boldsymbol{\tau}$ shows the

Cauchy stress tensor for incompressible viscuss fluids.

$$\tau = -P(I) + \mu A_1, \tag{2.47}$$

where

$$A_1 = \operatorname{grad} v + (\operatorname{grad} v)^t,$$

in which P is the pressure, A_1 is the first Rilvin-Erickson tensor, μ the dynamic viscosity and I the identity tensor.

2.20.3 Law of energy conservation

This law describes that the total energy is conserved in the whole system. Law of conservation of energy is also known as energy equation. For nanofluids, it is given by

$$\rho_f c_f \frac{DT}{Dt} = \tau.L^* + k\nabla^2 T + \rho_p c_p \left(D_B \nabla C.\nabla T + \frac{D_T}{T_\infty} \nabla T.\nabla T \right), \tag{2.48}$$

2.20.4 Law of conservation of concentration

For nanoparticles, the volume fraction equation is

$$\frac{\partial C}{\partial t} = -\frac{1}{\rho_p} \boldsymbol{\nabla}.\mathbf{j}_p, \tag{2.49}$$

or

$$\frac{\partial C}{\partial t} = \mathbf{D}_B \boldsymbol{\nabla}^2 \mathbf{C} + \mathbf{D}_T \frac{\boldsymbol{\nabla}^2 T}{T_\infty}. \tag{2.50}$$

2.21 Magnetohydrodynamics

The word magnetohydrodynamics (MHD) is the combination of three words magneto mean magnetic, hydro mean water or liquid and dynamics refer to the motion of an objects by forces. MHD describes the magnetic effects of electrically conducting fluids. Maxwell equations have an important role in MHD studies.

2.22 Mechanism of heat transfer

Heat is a type of energy which travels from hotter to colder region. Heat transfer process happen between two bodies which are put at various temperatures. The dispersion of heat happens by means of three main mechanisms, conduction, convection and radiation.

2.22.1 Conduction

The transfer of heat due to stimulation of molecules inside an object without any collective movement of the molecules within a material is specified as conduction. The process is generally carried out by the heat transfer in material molecule by molecule.

2.22.2 Radiation

The process of heat transfer without any medium is called radiation. The transfer of heat is merely due to the emission of electromagnetic waves. Combined effects of convection and radiation play significant role when heat transfer is considered in the liquids and gases.

2.22.3 Convection

Convection is the transport of heat due to surface movement of molecules. Such transformations occur between the solid material and the fluid.

2.23 Homotopy analysis method (HAM)

HAM technique is one of the best and simplest technique for obtaining convergent series solution for weakly as well as strongly non-linear equations. This method uses the concept of homotopy from topology. It is a continous mapping in which one function can be continuously converted into the other function, If one function f_1 and other function f_2 are maps from one topological space X into the other Y then there exist F such that

$$F : X \times [0, 1] \to Y, \tag{2.51}$$

where $x \in X$ and

$$F(x,0) = f_1(x),$$

$$F(x,1) = f_2(x). \tag{2.52}$$

F is known as homotopy.

Liao in 1992 used the homotopic technique for obtaining convergent series solution. HAM distinguishes itself from other techniques in the following ways:

1. It is independent of small/large parameter.

2. Convergent solution is guaranteed.

3. Freedom for the choice of base functions and linear operators.

2.24 Homotopic solutions

For the fundamental concept of homotopy analysis method, we assume a non-linear differential equation

$$\mathcal{N}\left[f\left(x\right)\right] = 0, \tag{2.53}$$

where $\mathcal{N}$ stands for non-linear operator, $f\left(x\right)$ for unknown function while x shows the independent variable. Zeroth-order problem is defined as follows:

$$\left(1 - Þ\right)\mathcal{L}\left[\tilde{f}\left(x; Þ\right) - f_0\left(x\right)\right] = Þ\hbar\mathcal{N}\left[\tilde{f}\left(x; Þ\right)\right], \tag{2.54}$$

in which $f_0\left(x\right)$ stands for the initial approximation, $\mathcal{L}$ is the auxiliary linear operator, $Þ \in [0,1]$ represents an embedding parameter, $\hbar$ for nonzero auxiliary parameter and $\tilde{f}\left(x; Þ\right)$ denotes the unknown function of x and Þ.

Setting $Þ = 0$ and $Þ = 1$, one has

$$\tilde{f}\left(x;0\right) = f_0\left(x\right) \quad \text{and} \quad \tilde{f}\left(x;1\right) = f\left(x\right). \tag{2.55}$$

The solution $\tilde{f}\left(x; Þ\right)$ varies from initial approximation $f_0\left(x\right)$ to the desired final solution $f\left(x\right)$

when Þ goes from 0 to 1. Using Taylor series expansion, we have

$$\tilde{f}\left(x;\text{Þ}\right)=f_0\left(x\right)+\sum_{m=1}^{\infty}f_m\left(x\right)\text{Þ}^m,\quad f_m\left(x\right)=\frac{1}{m!}\frac{\partial^m\tilde{f}\left(x;\text{Þ}\right)}{\partial\text{Þ}^m}\bigg|_{\text{Þ}=0}. \tag{2.56}$$

For Þ = 1, we get

$$f\left(x\right)=f_0\left(x\right)+\sum_{m=1}^{\infty}f_m\left(x\right). \tag{2.57}$$

Differentiating zeroth order equation m times, we get mth-order equation, and finally putting Þ = 0, we have the mth order equation

$$\mathcal{L}\left[f_m\left(x\right)-\chi_m f_{m-1}\left(x\right)\right]=\hbar\mathcal{R}_m\left(x\right), \tag{2.58}$$

$$\mathcal{R}_m\left(x\right)=\frac{1}{(m-1)!}\frac{\partial^m\mathcal{N}\left[\tilde{f}\left(x;\text{Þ}\right)\right]}{\partial\text{Þ}^m}\bigg|_{\text{Þ}=0}, \tag{2.59}$$

where

$$\chi_m=\begin{cases}0, & m\leq 1\\ 1, & m>1\end{cases}. \tag{2.60}$$

Chapter 3

An analytical solution for magnetohydrodynamic Oldroyd-B nanofluid flow induced by a stretching sheet with heat generation/absorption

3.1 Mathematical formulation:

We consider the three dimensional steady flow of an incompressible Oldroyd-B nanofluid flow towards a stretched surface. Flow analysis is performed in the existence of convective bounday condition. The $x-$ and $y-$axes are directed along the stretching surface while the $z-$axis is normal to it. Consider $u_w(x) = ax$ and $v_w(y) = by$ (where a, b are positve real numbers) are the stretching sheet velocities towards the $x-$ and $y-$ directions. Here, the stretching sheet velocities u and v differ linearly at the distance from the origin. Salient features of thermophoresis, Brownian motion and heat generation/absorption are added to the model.

The resulting boundary layer equations are given as:

$$u_x + v_y + w_z = 0, \tag{3.1}$$

$$uu_x + vu_y + wu_z + \lambda_1 \begin{pmatrix} u^2u_{xx} + v^2u_{yy} + w^2u_{zz} \\ +2uvu_{xy} + 2vwu_{yz} + 2uwu_{xz} \end{pmatrix}$$

$$= v \left(u_{zz} + \lambda_2 \begin{pmatrix} uu_{xzz} + vu_{yzz} + wu_{zzz} \\ -u_xu_{zz} - u_yv_{zz} - u_zw_{zz} \end{pmatrix} \right) - \frac{\sigma B_0^2}{\rho_f}(u + \lambda_1 wu_z), \tag{3.2}$$

$$uv_x + vv_y + wv_z + \lambda_1 \begin{pmatrix} u^2v_{xx} + v^2v_{yy} + w^2v_{zz} \\ +2uvv_{xy} + 2vwv_{yz} + 2uwv_{xz} \end{pmatrix}$$

$$= v \left(v_{zz} + \lambda_2 \begin{pmatrix} uv_{xzz} + vv_{yzz} + wv_{zzz} \\ -v_xu_{zz} - v_yv_{zz} - v_zw_{zz} \end{pmatrix} \right) - \frac{\sigma B_0^2}{\rho_f}(v + \lambda_1 wv_z), \tag{3.3}$$

$$uT_x + vT_y + wT_z = \alpha (T_{zz}) + \frac{Q}{(\rho c)_f} (T - T_\infty) + \tau \left(D_B (T_z C_z) + \frac{D_T}{T_\infty} (T_z)^2 \right), \tag{3.4}$$

$$uC_x + vC_y + wC_z = D_B (C_{zz}) + \frac{D_T}{T_\infty} (T_{zz}), \tag{3.5}$$

with suitable boundary conditions

$$u = ax,\ v = by,\ w = 0,$$

$$-K (T_z) = h_f (T_f - T), \quad D_B (C_z) + \frac{D_T}{T_\infty} (T_z) = 0 \ \text{ at } \ z = 0,$$

$$u \to 0,\ v \to 0,\ T \to T_\infty,\ C \to C_\infty \ \text{ as } \ z \to \infty. \tag{3.6}$$

Dimensionless form of above mathematical model is obtained by using following transformations:

$$\eta = \sqrt{\frac{a}{\nu}} z, \quad \theta (\eta) = \frac{T - T_\infty}{T_f - T_\infty}, \quad \phi (\eta) = \frac{C - C_\infty}{C_\infty},$$

$$u = axf' (\eta), \quad v = ayg' (\eta), \quad w = -(av)^{1/2} (f (\eta) + g (\eta)). \tag{3.7}$$

Here, satisfaction of Eq. (3.1) is inevitable. However, Eqs. $(3.2-3.5)$ take the form

$$f''' + \left(M^2\beta_1 + 1\right)(f+g)\,f'' - f'^2 + \beta_1\left(2\,(f+g)\,f'f'' - (f+g)^2\,f'''\right)$$
$$+\beta_2\left(\left(f'' + g''\right)f'' - (f+g)\,f''''\right) - M^2 f' = 0, \tag{3.8}$$

$$g''' + \left(M^2\beta_1 + 1\right)(f+g)\,g'' - g'^2 + \beta_1\left(2\,(f+g)\,g'g'' - (f+g)^2\,g'''\right)$$
$$+\beta_2\left(\left(f'' + g''\right)g'' - (f+g)\,g''''\right) - M^2 g' = 0, \tag{3.9}$$

$$\theta'' + \Pr\,(f+g)\,\theta' + \Pr\,S\theta + \Pr\,Nb\theta'\phi' + \Pr\,Nt\theta'^2 = 0, \tag{3.10}$$

$$\phi'' + Sc\,(f+g)\,\phi' + \frac{Nt}{Nb}\theta'' = 0, \tag{3.11}$$

$$f = g = 0, \quad f' = 1, \quad g' = \lambda, \quad \theta' = -\gamma\,(1-\theta\,(0))\,, \quad Nb\phi' + Nt\theta' = 0 \ \text{ at } \eta = 0,$$

$$f' \to 0, \quad g' \to 0, \ \theta \to 0, \quad \phi \to 0 \ \text{ at } \eta \to \infty. \tag{3.12}$$

These quantities are defined as follows:

$$\beta_1 = \lambda_1 a, \ \beta_2 = \lambda_2 a, \ M^2 = \frac{\sigma B_0^2}{\rho_f a}, \ \lambda = \frac{b}{a}, \ \Pr = \frac{\nu}{\alpha}, \ S = \frac{Q}{a\,(\rho c)_f},$$
$$Nb = \frac{\tau D_B C_\infty}{\nu}, \ Nt = \frac{\tau D_T\,(T_f - T_\infty)}{\nu T_\infty}, \ Sc = \frac{\nu}{D_B}, \ \gamma = \frac{h_f}{K}\sqrt{\frac{\nu}{a}}. \tag{3.13}$$

The local Nusselt number Nu_x is given by

$$Nu_x = -\frac{x}{(T_w - T_\infty)}\,(T_z)\,|_{z=0} = -\,(\mathrm{Re}_x)^{1/2}\,\theta'\,(0)\,. \tag{3.14}$$

It can be noted that the non-dimensional mass flux represented by a Sherwood number Sh_x is now identically zero. Where $\mathrm{Re}_x = U_w x/v$ shows the local Reynolds number.

.

3.2 Homopotic solutions

Following this method, the initial guesses $(f_0, g_0\ , \theta_0, \ \phi_0)$ and linear operators $(\mathcal{L}_f, \mathcal{L}_g, \ \mathcal{L}_\theta, \ \mathcal{L}_\phi)$ are selected are given as follows:

$$f_0(\eta) = (1 - \exp(-\eta)),\ g_0 = \lambda(1 - \exp(-\eta)),\ \theta_0(\eta) = \frac{\gamma}{1+\gamma}\exp(-\eta),$$

$$\phi_0(\eta) = -\frac{\gamma}{1+\gamma}\frac{Nt}{Nb}\exp(-\eta), \tag{3.15}$$

$$\mathcal{L}_f = f''' - f', \mathcal{L}_g = g''' - g',\ \mathcal{L}_\theta = \theta'' - \theta,\ \mathcal{L}_\phi = \phi'' - \phi, \tag{3.16}$$

with the properties

$$\mathcal{L}_f\left[B_1 + B_2\exp(\eta) + B_3\exp(-\eta)\right] = 0,$$

$$\mathcal{L}_g\left[B_4 + B_5\exp(\eta) + B_6\exp(-\eta)\right] = 0,$$

$$\mathcal{L}_\theta\left[B_7\exp(\eta) + B_8\exp(-\eta)\right] = 0,$$

$$\mathcal{L}_\phi\left[B_9\exp(\eta) + B_{10}\exp(-\eta)\right] = 0, \tag{3.17}$$

where B_j $(j = 1 - 10)$ are the arbitrary constants.

3.2.1 Zeroth and mth order deformation problems

The zeroth order deformation problem is defined as,

$$(1-p)\mathcal{L}_f\left[\widehat{f}(\eta;p) - f_0(\eta)\right] = p\hbar_f\mathcal{N}_f\left[\widehat{f}(\eta;p), \widehat{g}(n,p)\right], \tag{3.18}$$

$$(1-p)\mathcal{L}_g\left[\widehat{g}(\eta;p) - g_0(\eta)\right] = p\hbar_g\mathcal{N}_g\left[\widehat{f}(\eta;p), \widehat{g}(n,p)\right], \tag{3.19}$$

$$(1-p)\mathcal{L}_\theta\left[\widehat{\theta}(\eta;p) - \theta_0(\eta)\right] = p\hbar_\theta\mathcal{N}_\theta\left[\widehat{f}(\eta;p), \widehat{g}(n,p), \widehat{\theta}(\eta;p), \widehat{\phi}(\eta;p)\right], \tag{3.20}$$

$$(1-p)\mathcal{L}_\phi\left[\widehat{\phi}(\eta;p) - \phi_0(\eta)\right] = p\hbar_\phi\mathcal{N}_\phi\left[\widehat{f}(\eta;p), \widehat{g}(n,p), \widehat{\theta}(\eta;p), \widehat{\phi}(\eta;p)\right], \tag{3.21}$$

$$\widehat{f}(0;p) = 0, \quad \widehat{f}'(0;p) = 1, \quad \widehat{f}'(\infty;p) = 0,$$

$$\widehat{g}(0;p) = 0, \quad \widehat{g}'(0;p) = 1, \quad \widehat{g}'(\infty;p) = 0,$$

$$\widehat{\theta}(0;p) = -\gamma\left(1 - \widehat{\theta}(0,p)\right), \quad \widehat{\theta}(\infty;p) = 0,$$

$$Nb\widehat{\phi}(0;p) + Nt\widehat{\phi'}(0;p) = 0, \quad \widehat{\phi}(\infty;p) = 0,$$

$$\mathcal{N}_f\left[\widehat{f}(\eta;p),\widehat{g}(\eta;p)\right]=\frac{\partial^3\widehat{f}(\eta;p)}{\partial\eta^3}+\left(1+M^2\beta_1\right)\left(\widehat{f}+\widehat{g}\right)\frac{\partial^2\widehat{f}(\eta;p)}{\partial\eta^2}-\left(\frac{\partial\widehat{f}(\eta;p)}{\partial\eta}\right)^2-M^2\frac{\partial\widehat{f}(\eta;p)}{\partial\eta}$$

$$+\beta_1\begin{pmatrix}2\left(\widehat{f}+\widehat{g}\right)\frac{\partial\widehat{f}(\eta;p)}{\partial\eta}\frac{\partial^2\widehat{f}(\eta;p)}{\partial\eta^2}\\-\left(\widehat{f}+\widehat{g}\right)^2\frac{\partial^3\widehat{f}(\eta;p)}{\partial\eta^3}\end{pmatrix}+\beta_2\begin{pmatrix}\left(\frac{\partial^2\widehat{f}(\eta;p)}{\partial\eta^2}+\frac{\partial^2\widehat{g}(\eta;p)}{\partial\eta^2}\right)\frac{\partial^2\widehat{f}(\eta;p)}{\partial\eta^2}\\-\left(\widehat{f}+\widehat{g}\right)\frac{\partial^4\widehat{f}(\eta;p)}{\partial\eta^4}\end{pmatrix},\tag{3.22}$$

$$\mathcal{N}_g\left[\widehat{f}(\eta;p),\widehat{g}(\eta;p)\right]=\frac{\partial^3\widehat{g}(\eta;p)}{\partial\eta^3}+\left(1+M^2\beta_1\right)\left(\widehat{f}+\widehat{g}\right)\frac{\partial^2\widehat{g}(\eta;p)}{\partial\eta^2}-\left(\frac{\partial\widehat{g}(\eta;p)}{\partial\eta}\right)^2-M^2\frac{\partial\widehat{g}(\eta;p)}{\partial\eta}$$

$$+\beta_1\begin{pmatrix}2\left(\widehat{f}+\widehat{g}\right)\frac{\partial\widehat{g}(\eta;p)}{\partial\eta}\frac{\partial^2\widehat{g}(\eta;p)}{\partial\eta^2}\\-\left(\widehat{f}+\widehat{g}\right)^2\frac{\partial^3\widehat{g}(\eta;p)}{\partial\eta^3}\end{pmatrix}+\beta_2\begin{pmatrix}\left(\frac{\partial^2\widehat{f}(\eta;p)}{\partial\eta^2}+\frac{\partial^2\widehat{g}(\eta;p)}{\partial\eta^2}\right)\frac{\partial^2\widehat{g}(\eta;p)}{\partial\eta^2}\\-\left(\widehat{f}+\widehat{g}\right)\frac{\partial^4\widehat{g}(\eta;p)}{\partial\eta^4}\end{pmatrix},\tag{3.23}$$

$$\mathcal{N}_\theta\left[\widehat{f}(\eta;p),\widehat{g}(n,p),\widehat{\theta}(\eta;p),\widehat{\phi}(\eta;p)\right]=\frac{1}{\mathrm{Pr}}\frac{\partial^2\widehat{\theta}(\eta,p)}{\partial\eta^2}+\left(\widehat{f}+\widehat{g}\right)\frac{\partial\widehat{\theta}(\eta,p)}{\partial\eta}+S\widehat{\theta}$$

$$+Nb\frac{\partial\widehat{\theta}(\eta;p)}{\partial\eta}\frac{\partial\widehat{\phi}(\eta;p)}{\partial\eta}+Nt\left(\frac{\partial\widehat{\theta}(\eta,p)}{\partial\eta}\right)^2,\tag{3.24}$$

$$\mathcal{N}_\phi\left[\widehat{f}(\eta;p),\widehat{g}(n,p),\widehat{\theta}(\eta;p),\widehat{\phi}(\eta;p)\right]=\frac{1}{Sc}\frac{\partial^2\widehat{\phi}(\eta,p)}{\partial\eta^2}+\left(\widehat{f}+\widehat{g}\right)\frac{\partial\widehat{\phi}(\eta,p)}{\partial\eta}$$

$$+\frac{N_t}{N_B}\frac{1}{Sc}\frac{\partial^2\widehat{\theta}(\eta,p)}{\partial\eta^2},\tag{3.25}$$

where $p\in[0,1]$ is embedding parameter and $\hbar_f,\hbar_g,\hbar_\theta$ and $\hbar_\phi$ are the non-zero auxiliary parameters.

3.2.2 mth-order deformation problems

Here, we have

$$\mathcal{L}_f\left[f_m(\eta)-\chi_m f_{m-1}(\eta)\right]=\hbar_f\mathcal{R}_f^m(\eta),\tag{3.26}$$

$$\mathcal{L}_g\left[g_m(\eta)-\chi_m g_{m-1}(\eta)\right]=\hbar_f\mathcal{R}_g^m(\eta),\tag{3.27}$$

$$\mathcal{L}_\theta \left[\theta_m \left(\eta\right) - \chi_m \theta_{m-1} \left(\eta\right)\right] = \hbar_\theta \mathcal{R}_\theta^m \left(\eta\right), \tag{3.28}$$

$$\mathcal{L}_\phi \left[\phi_m \left(\eta\right) - \chi_m \phi_{m-1} \left(\eta\right)\right] = \hbar_\phi \mathcal{R}_\phi^m \left(\eta\right), \tag{3.29}$$

$$f_m \left(0\right) = \ f_m^{'} \left(0\right) = f_m^{'} \left(\infty\right) = 0, \ g_m \left(0\right) = g_m^{'} \left(0\right) = g_m^{'} \left(\infty\right) = 0, \tag{3.30}$$

$$\theta_m \left(0\right) - \gamma \theta_m \left(0\right) = 0, \theta_m \left(\infty\right) = 0, Nb\phi_m \left(0\right) + Nt\theta_m \left(0\right) = 0, \phi_m \left(\infty\right) = 0. \tag{3.31}$$

$$\mathcal{R}_f^m \left(\eta\right) = f_{m-1}^{'''} - M^2 f_{m-1}^{'} + \left(1 + M^2 \beta_1\right) \sum_{k=0}^{m-1} \left(f_{m-1-k} + g_{m-1-k}\right) f_k^{''} - \sum_{k=0}^{m-1} f_{m-1-k}^{'} f_k^{'}$$

$$+2\beta_1 \sum_{k=0}^{m-1} f_{m-1-k} \sum_{l=0}^{k} f_{k-1}^{'} f_1^{''} + 2\beta_1 \sum_{k=0}^{m-1} g_{m-1-k} \sum_{l=0}^{k} f_{k-1}^{'} f_1^{''} - \beta_1 \sum_{k=0}^{m-1} f_{_{m-1-k}} \sum_{l=0}^{k} f_{k-1} f_1^{'''}$$

$$-\beta_1 \sum_{k=0}^{m-1} g_{m-1-k} \sum_{l=0}^{k} g_{k-1} f_1^{'''} - 2\beta_1 \sum_{k=0}^{m-1} g_{m-1-k} \sum_{l=0}^{k} f_{k-1} f_1^{'''}$$

$$+\beta_2 \sum_{k=0}^{m-1} \left(f_{m-1-k}^{''} + g_{m-1-k}^{''}\right) f_k^{''} - \beta_2 \sum_{k=0}^{m-1} \left(f_{m-1-k} + g_{m-1-k}\right) f_k^{iv}, \tag{3.32}$$

$$\mathcal{R}_g^m \left(\eta\right) = g_{m-1}^{'''} - M^2 g_{m-1}^{'} + \left(1 + M^2 \beta_1\right) \sum_{k=0}^{m-1} \left(f_{m-1-k} + g_{m-1-k}\right) g_k^{''} - \sum_{k=0}^{m-1} g_{m-1-k}^{'} g_k^{'}$$

$$+2\beta_1 \sum_{k=0}^{m-1} f_{m-1-k} \sum_{l=0}^{k} g_{k-1}^{'} g_1^{''} + 2\beta_1 \sum_{k=0}^{m-1} g_{m-1-k} \sum_{l=0}^{k} g_{k-1}^{'} g_1^{''} - \beta_1 \sum_{k=0}^{m-1} f_{m-1-k} \sum_{l=0}^{k} f_{k-1} g_1^{'''}$$

$$-\beta_1 \sum_{k=0}^{m-1} g_{m-1-k} \sum_{l=0}^{k} g_{k-1} g_1^{'''} - 2\beta_1 \sum_{k=0}^{m-1} g_{m-1-k} \sum_{l=0}^{k} f_{k-1} g_1^{'''}$$

$$+\beta_2 \sum_{k=0}^{m-1} \left(f_{m-1-k}^{''} + g_{m-1-k}^{''}\right) g_k^{''} - \beta_2 \sum_{k=0}^{m-1} \left(f_{m-1-k} + g_{m-1-k}\right) g_k^{iv}, \tag{3.33}$$

$$\mathcal{R}_{\theta}^{m}(\eta)=\frac{1}{\Pr}\theta_{m-1}''+\sum_{k=0}^{m-1}\left(f_{m-1-k}\theta_{k}'+g_{m-1-k}\theta_{k}'\right)+S\theta_{m-1}$$

$$+Nb\sum_{k=0}^{m-1}\theta_{m-1-k}'\phi_{k}'+Nt\sum_{k=0}^{m-1}\theta_{m-1-k}'\theta_{k}', \tag{3.34}$$

$$\mathcal{R}_{\phi}^{m}(\eta)=\frac{1}{Sc}\phi_{m-1}''+\sum_{k=0}^{m-1}\left(f_{m-1-k}\phi_{k}'+g_{m-1-k}\phi_{k}'\right)+S\theta_{m-1}+\frac{Nt}{Nb}\frac{1}{Sc}\theta_{m-1}'', \tag{3.35}$$

$$\chi_{m}=\begin{cases}0, & m\leq 1\\ 1, & m>1\end{cases}. \tag{3.36}$$

The general solutions $(f_m, g_m, \theta_m, \phi_m)$ of Eqs. $(3.26-3.29)$ in terms of special solutions $(f_m^*, g_m^*, \theta_m^*, \phi_m^*)$ are given by

$$f_{m}(\eta)=f_{m}^{\star}(\eta)+B_{1}+B_{2}e^{\eta}+B_{3}e^{-\eta}, \tag{3.37}$$

$$g_{m}(\eta)=g_{m}^{\star}(\eta)+B_{4}+B_{5}e^{\eta}+B_{6}e^{-\eta}, \tag{3.38}$$

$$\theta_{m}(\eta)=\theta_{m}^{\star}(\eta)+B_{7}e^{\eta}+B_{8}e^{-\eta}, \tag{3.39}$$

$$\phi_{m}(\eta)=\phi_{m}^{\star}(\eta)+B_{9}e^{\eta}+B_{10}e^{-\eta}, \tag{3.40}$$

where the constants B_j $(j=1-10)$ through the boundary conditions (3.30) and (3.31) have the values

$$B_{2}=B_{5}=B_{7}=B_{9}=0,\quad B_{3}=\frac{\partial f_{m}^{\star}(\eta)}{\partial\eta}_{\eta=0},\ B_{1}=-B_{3}-f_{m}^{\star}(0), \tag{3.41}$$

$$B_{6}=\frac{\partial g_{m}^{\star}(\eta)}{\partial\eta}_{\eta=0},\ B_{4}=-B_{6}-g_{m}^{\star}(0), B_{8}=\frac{1}{1+\gamma}\left(\frac{\partial\theta_{m}^{\star}(\eta)}{\partial\eta}_{\eta=0}-\gamma\theta_{m}^{\star}(0)\right), \tag{3.42}$$

$$B_{10}=\frac{\partial\phi_{m}^{\star}(\eta)}{\partial\eta}_{\eta=0}+\frac{Nt}{Nb}\left(-B_{8}+\frac{\partial\theta_{m}^{\star}(\eta)}{\partial\eta}_{\eta=0}\right). \tag{3.43}$$

3.3 Convergence analysis

Homotopy analysis technique is used for the series solutions of highly nonlinear problems which depends on auxiliary parameters $\hbar_f, \hbar_g, \hbar_\theta$ and $\hbar_\phi$. These parameters are essential to adjust and control the convergence region of series solutions. Therefore, we have plotted the $\hbar$-curves in the Fig. 3.1. The admissible ranges of the auxiliary parameters $\hbar_f, \hbar_g, \hbar_\theta$ and $\hbar_\phi$ are $-1.1 \leq \hbar_f \leq 0.0$, $-1.2 \leq \hbar_g \leq -0.1$, $-1.4 \leq \hbar_\theta \leq -0.2$ and $-2.2 \leq \hbar_\phi \leq -0.6$ when $\gamma = 0.5$, $\lambda = 0.2$, $Pr = 1.2$, $M = 0.1$, $S = 0.1$, $Sc = 1.0$, $\beta_1 = 0.2$, $\beta_2 = 0.2$, $Nt = 0.3$ and $Nb = 0.5$. Table 3.1 shows the convergenc of series solutions of momentum, energy and concentration equations and it illustrates that the 20th order of guesstimate are adequate for the convergent series solutions which are in good agreement to graphical illustration shown in Fig. 3.1.

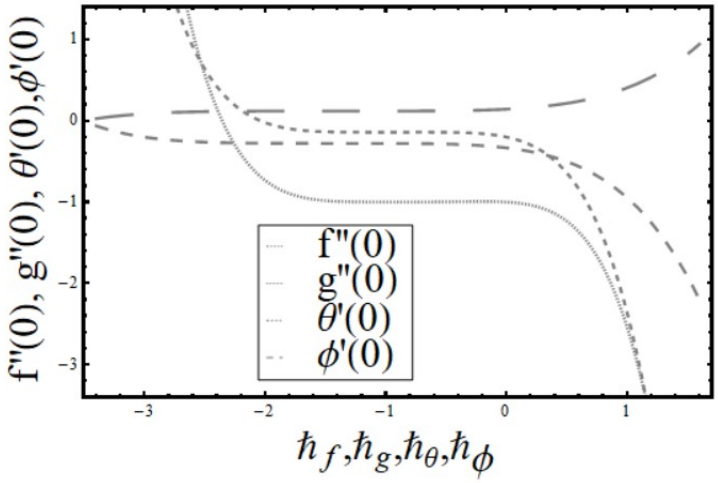

Fig. 3.1. $\hbar-$curves for f, g, θ and ϕ

Table 3.1: Convergence of homotopic solutions for various order of approximations when

and $\hbar_f = \hbar_g = -0.9 = \hbar_\theta = \hbar_\phi$

Order of Approximations	$-f''(0)$	$-g'(0)$	$-\theta'(0)$	$-\phi(0)$
1	0.98446	0.14313	0.30133	0.12914
5	0.99954	0.14070	0.28238	0.12102
10	0.99936	0.14123	0.27932	0.11971
20	0.99927	0.14125	0.27902	0.11958
25	0.99927	0.14125	0.27902	0.11958

3.4 Results and discussion

The present segment elucidates the impact of different various parameters like the Deborah numbers in terms of relaxation and retardation times β_1 and β_2 respectively, ratio parameter λ, magnetic parameter M, Biot number γ, Schmidt number Sc, Prandtl number Pr, heat generation/absorption parameter S, Brownian motion parameter Nb and thermophoresis parameter Nt on the dimensionless velocity components $f'(\eta)$, $g'(\eta)$, temperature $\theta(\eta)$ and nanoparticles concentration $\phi(\eta)$ distributions. Figure 3.2 is plotted to examine the behavior of Deborah number β_1 on the velocity profile $f'(\eta)$. It is seen that for large values of Deborah number β_1 velocity profile decreases. Figure 3.3 depicted the effect of Deborah number β_2 on the velocity profile $f'(\eta)$. Both velocity $f'(\eta)$ and thickness of the thermal layer are higher for increasing values of Deborah number β_2. A parallel investigation of figure 3.2 and 3.3 surely indicates that β_1 and β_2 have fully different behaviors on the velocity profile $f'(\eta)$. Here β_1 concerns the relaxation time although β_2 depends on the retardation time. As β_1 and β_2 increase, it correspond to greater relaxation and retardation times respectively. Greater relaxation time causes to a weaker velocity profile although retardation time leads to a stronger velocity profile. Moreover, the recent analysis reduce to the Maxwell fluid flow case when $\beta_2 = 0$. Figure 3.4 is portrayed to see the impact of magnetic parameter M on velocity profile $g'(\eta)$. Magnetic parameter M associates the Lorentz force. It decreases with the increasing value of magnetic parameter M. Figure 3.5 shows the variation in velocity profile $g'(\eta)$ for various values of Deborah number β_2. Both the velocity and thickness of the thermal layer are higher for increasing values of Deborah number β_2. Figure 3.6 is plotted to examine the behavior of Deborah number

β_1 on the temperature profile $\theta(\eta)$. Both the thickness of the thermal layer and temperature $\theta(\eta)$ are greater for increasing values of Deborah number β_1. Figure 3.7 indicates that an increase in Deborah number β_2 effects a decay in temperature profile $\theta(\eta)$ and in associated thickness of thermal layer. Figure 3.8 shows that an increment in ratio parameter λ corresponds to a weaker temperature profile $\theta(\eta)$ and low thickness of thermal layer. For $\lambda = 0$, two-dimensional flow situation is obtained. Influence of magnetic parameter M on the temperature profile $\theta(\eta)$ is plotted in Figure 3.9. Both the thickness of thermal layer and temperature $\theta(\eta)$ are increased for greater values of magnetic parameter M. As magnetic parameter M associates the Lorentz force. Greater values of magnetic parameter M corresponds to a stronger Lorentz force which causes an increment in related thickness of thermal layer and temperature profile. Here $M = 0$, leads to a hydrodynamic flow situation. Change in temperature profile $\theta(\eta)$ for various values of Biot number γ is plotted in Figure 3.10. Here, thickness of thermal layer and temperature $\theta(\eta)$ indicates an increasing behavior for greater values of Biot number γ. Greater values of Biot number leads to stronger convection although yields a more thickness of thermal layer and higher temperature profile. Figure 3.11 indicates that variations in temperature profile $\theta(\eta)$ for distinct values of heat generation/absorption parameter. Here, $S > 0$, leads to heat generation and $S < 0$, corresponds to heat absorption. It is surely seen that temperature profile $\theta(\eta)$ and thickness of thermal layer are higher in the case of heat generation as compare to the heat absorption case. Figure 3.12 displays that thickness of thermal boundary layer and temperature profile $\theta(\eta)$ are decreasing functions of Prandtl number Pr. There is an inverse relationship with Prandtl number Pr and thermal diffusivity. An increment in Prandtl number Pr, corresponds to lower thermal diffusivity which causes decay in the temperature profile and thickness of thermal layer. Figure 3.13 is sketched to portray the behavior of thermophoresis parameter Nt on temperature profile $\theta(\eta)$. Both temperature $\theta(\eta)$ and thickness of thermal layer are increased for growing values of thermophoresis parameter Nt. Greater values of thermophoresis parameter Nt cause an increment in the thermophoresis force which leads to move nanoparticles from hot to cold surfaces and similarly it increases the temperature and thickness of thermal layer. Figure 3.14 presents the effects of Deborah number β_1 on nanoparticles concentration profile $\phi(\eta)$. Greater values of Deborah number β_1 causes an increment in nanoparticles concentration profile. Change in nanoparticles concentra-

tion field $\phi(\eta)$ for different values of Deborah number β_2 is plotted in figure 3.15. Both the thickness of nanoparticles concentration layer and nanoparticles concentration field are weaker for increasing values of Deborah number β_2. Impact of ratio parameter λ on nanoparticles concentration profile $\phi(\eta)$ is displayed in figure 3.16. An increment in ratio parameter λ causes decay in nanoparticles concentration profile $\phi(\eta)$. Figure 3.17 indicates that greater values of magnetic parameter M corresponds to higher nanoparticles concentration profile and more thickness of nanoparticles concentration layer. Figure 3.18 shows the behavior of Biot number γ on nanoparticles concentration profile $\phi(\eta)$. Here nanoparticles concentration profile $\phi(\eta)$ and thickness of nanoparticles concentration layer are increasing functions of Biot number γ. Effect of thermophoresis parameter Nt on nanoparticles concentration profile $\phi(\eta)$ is drawn in figure 3.19. Greater values of thermophoresis parameter Nt cause an enhancement in the thermophoresis force which leads to move nanoparticles from hot to cold surfaces. Figure 3.20 elucidates that an increase in Schmidt number Sc corresponds to decay in nanoparticles concentration distribution $\phi(\eta)$. There is an inverse relationship between Schmidt number and the Brownian diffusion coefficient. Greater values of Schmidt number Sc leads to a lower Brownian diffusion coefficient, which causes reduction in nanoparticles concentration distribution. Figure 3.21 depicts that greater values of Brownian motion parameter Nb leads to the weaker nanoparticles concentration profile $\phi(\eta)$ and shows the low thickness of the nanoparticles concentration layer. Table 3.2 shows numerical values of local Nusselt number $-\theta'(0)$ for various values of β_1, β_2, λ, S, γ, Nt, Nb, Sc, Pr and M. It is observed that values of local Nusselt number are higher for increasing values of Biot γ and Prandtl Pr numbers while the opposite behavior is seen for thermophoresis parameter Nt. It can also be noticed that the impacts of β_1 and β_2, on the local Nusselt number are quite reversed. Furthermore, the values of local Nusselt number are greater for the hydrodynamic flow case ($M = 0$)when compared with the hydromagnetic flow situation ($M \neq 0$).

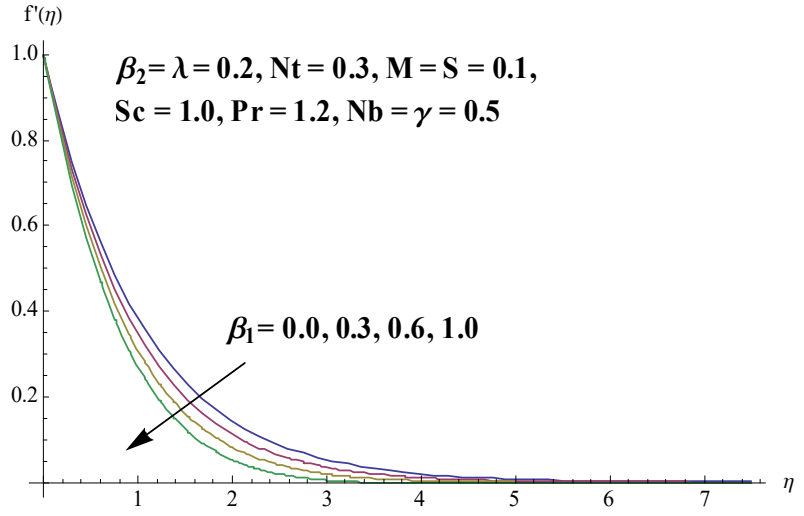

Fig. 3.2: Influence of Deborah number β_1 on velocity profile $f'(\eta)$.

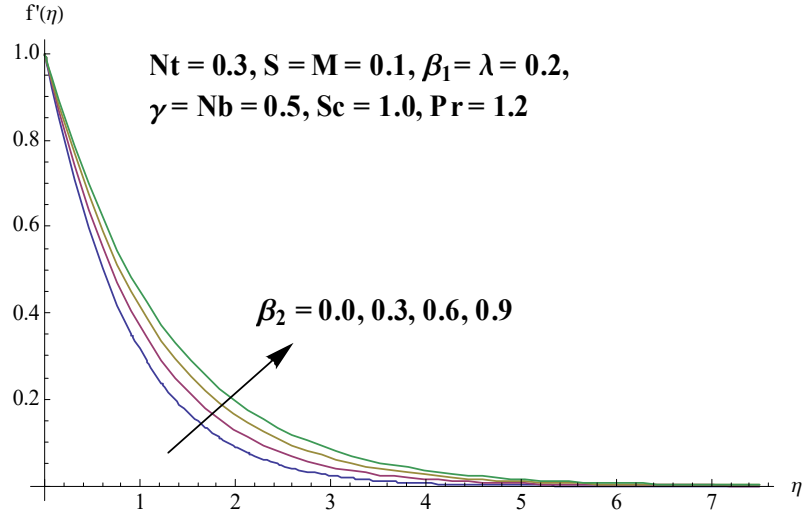

Fig. 3.3: Influence of Deborah number β_2 on velocity profile $f'(\eta)$.

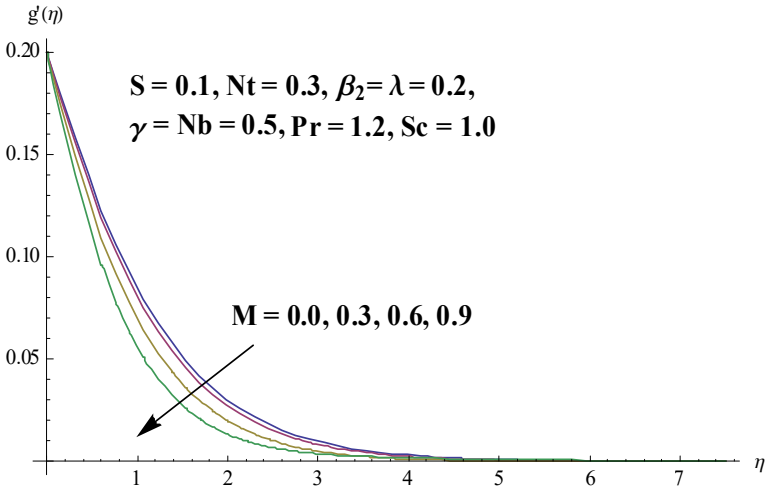

Fig. 3.4: Influence of magnetic parameter M on velocity profile $g'(\eta)$.

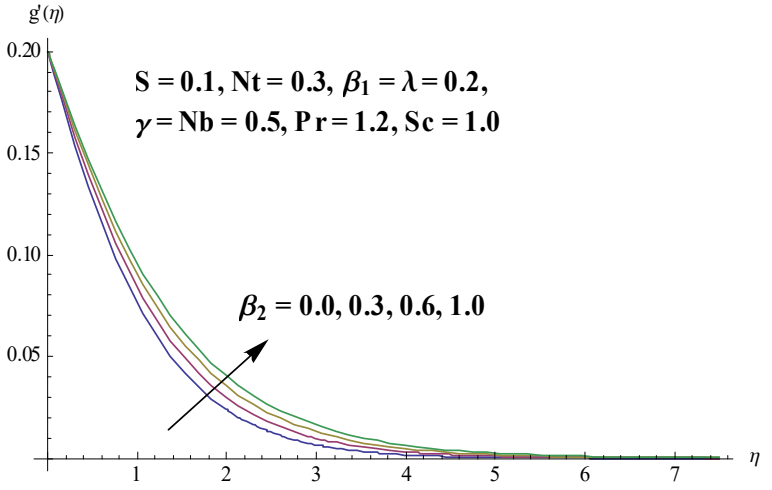

Fig. 3.5: Influence of Deborah number β_2 on velocity profile $g'(\eta)$.

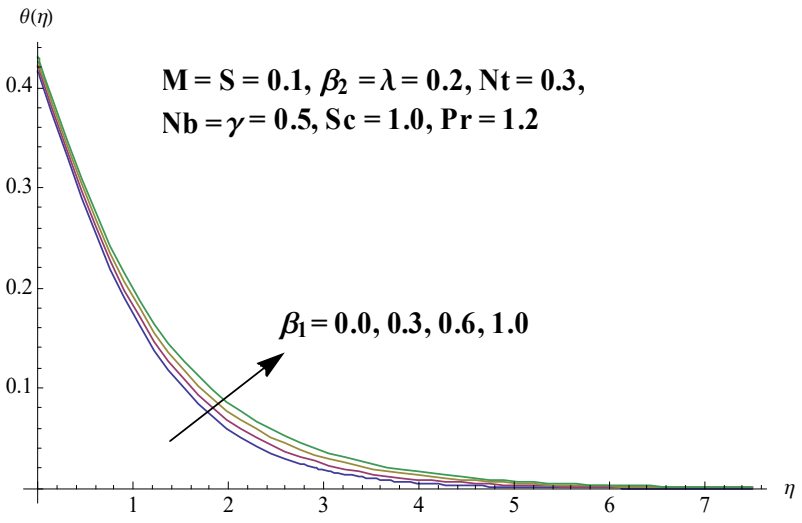

Fig. 3.6: Influence of Deborah number β_1 on temperature profile $\theta(\eta)$.

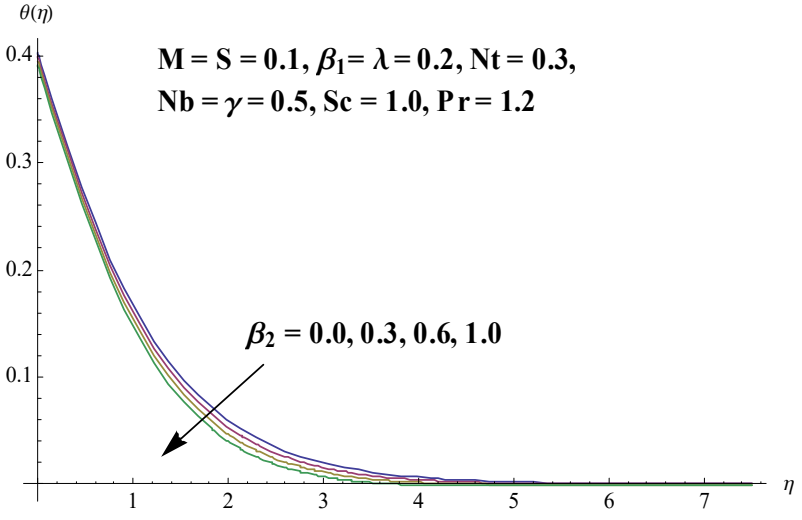

Fig. 3.7: Influence of Deborah number β_2 on temperature profile $\theta(\eta)$.

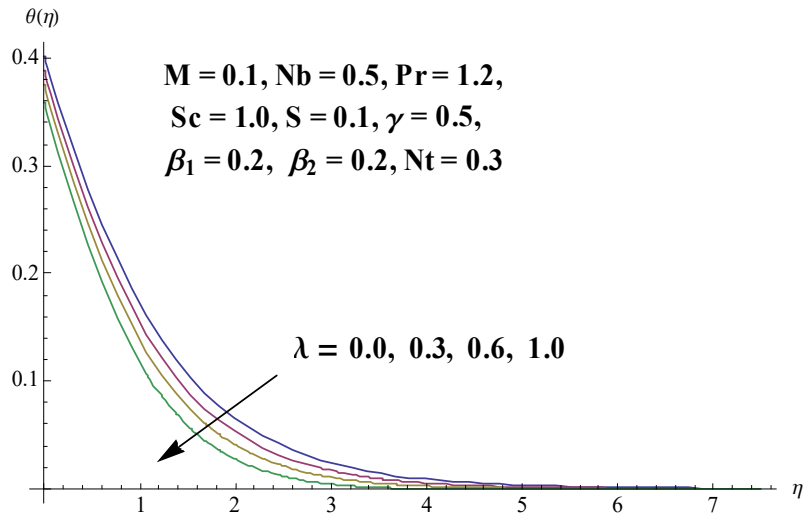

Fig. 3.8: Influence of ratio parameter λ on temperature profile $\theta(\eta)$.

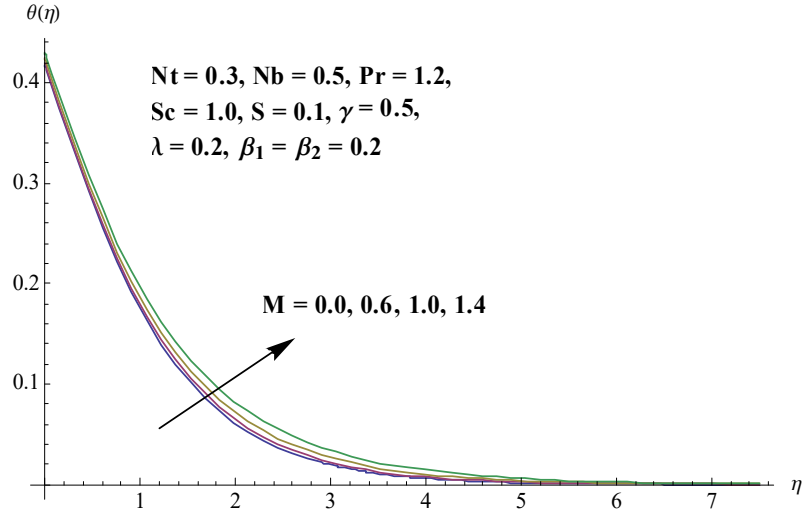

Fig. 3.9: Influence of magnetic parameter M on temperature profile $\theta(\eta)$.

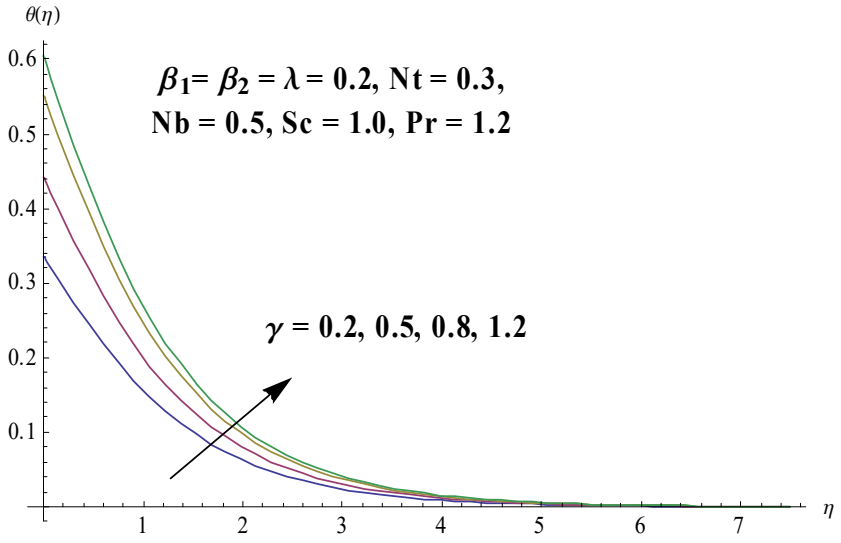

Fig. 3.10: Influence of Biot number γ on temperature profile $\theta(\eta)$.

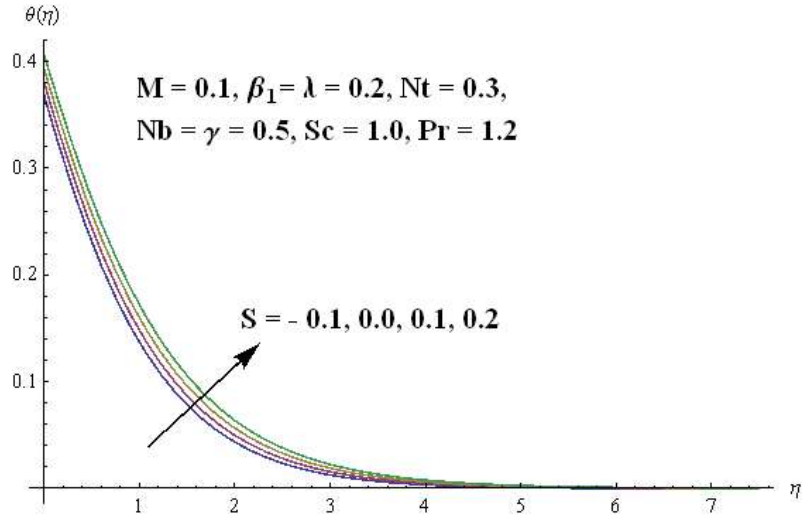

Fig. 3.11: Influence of heat generation/absorption parameter S on $\theta(\eta)$.

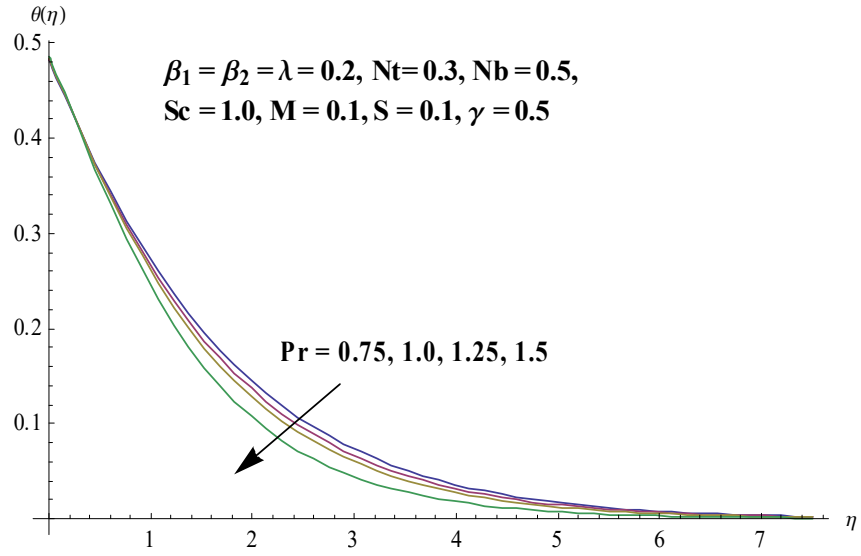

Fig. 3.12: Influence of Prandtl number Pr on temperature profile $\theta(\eta)$.

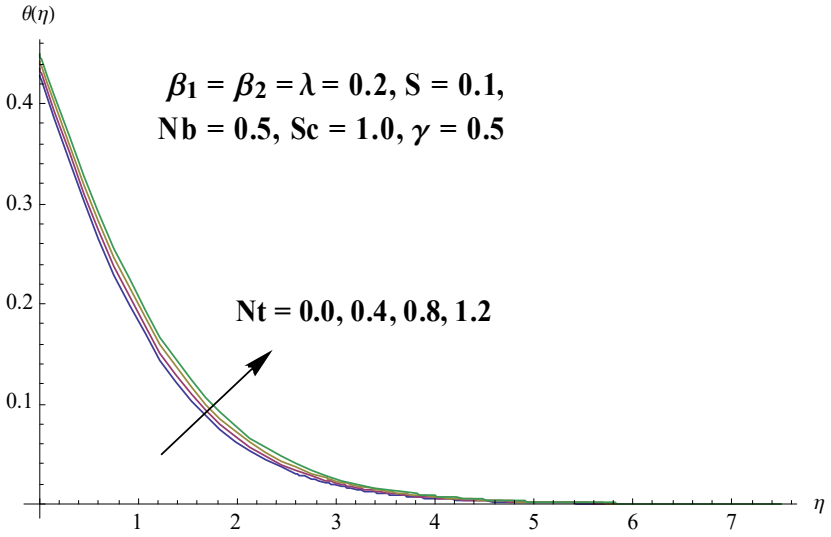

Fig. 3.13: Influence of thermophoresis parameter Nt on temperature profile $\theta(\eta)$.

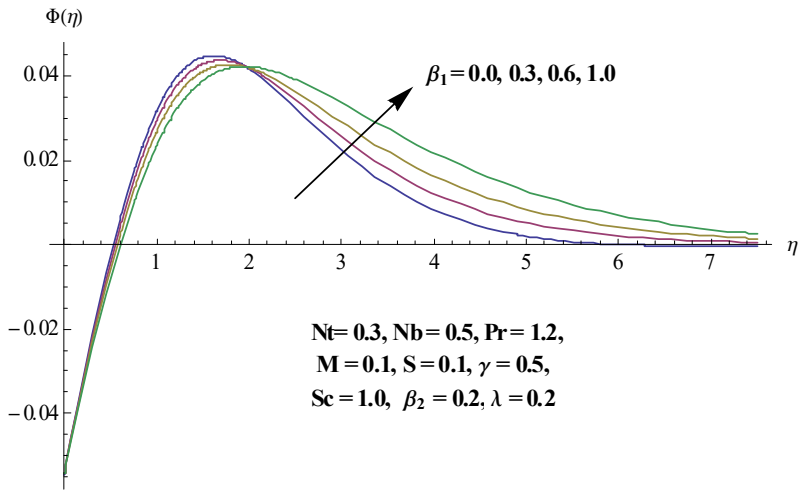

Fig. 3.14: Influence of Deborah number β_1 on concentration profile $\phi(\eta)$.

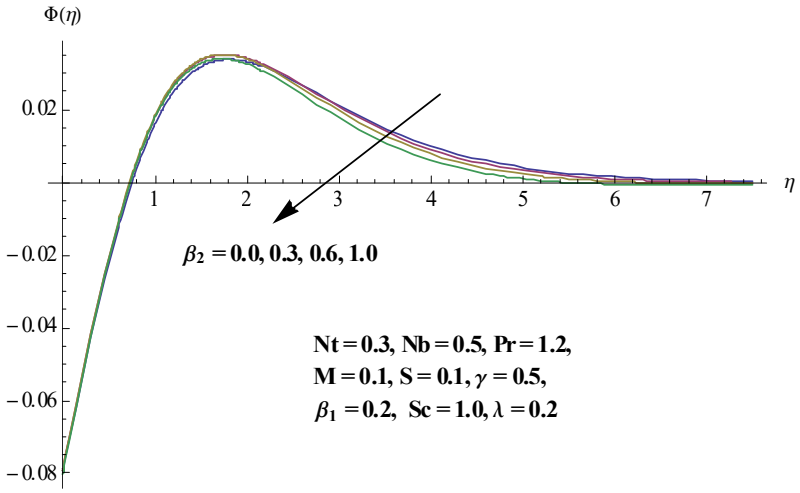

Fig. 3.15: Influence of Deborah number β_2 on concentration profile $\phi(\eta)$.

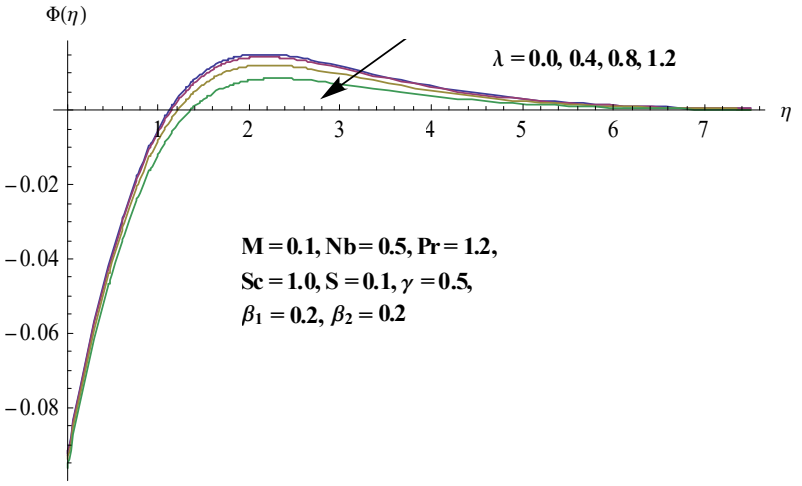

Fig. 3.16: Influence of ratio parameter λ on concentration profile $\phi(\eta)$.

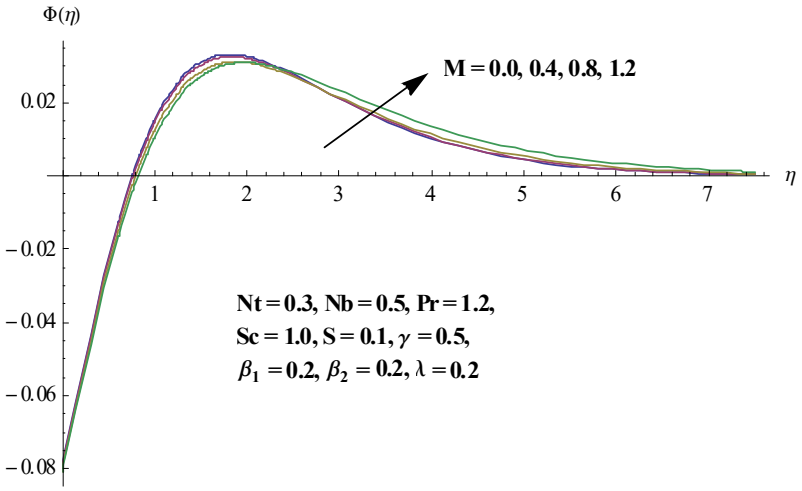

Fig. 3.17: Influence of magnetic parameter M on concentration profile $\phi(\eta)$.

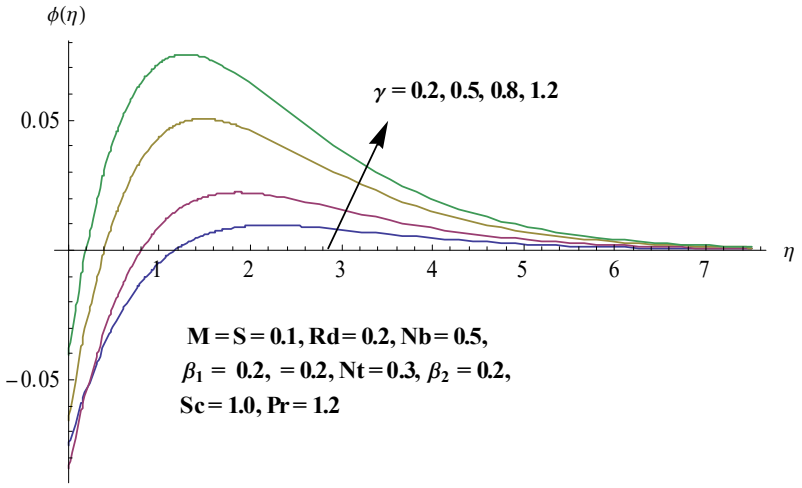

Fig. 3.18: Influence of Biot number γ on concentration profile $\phi(\eta)$.

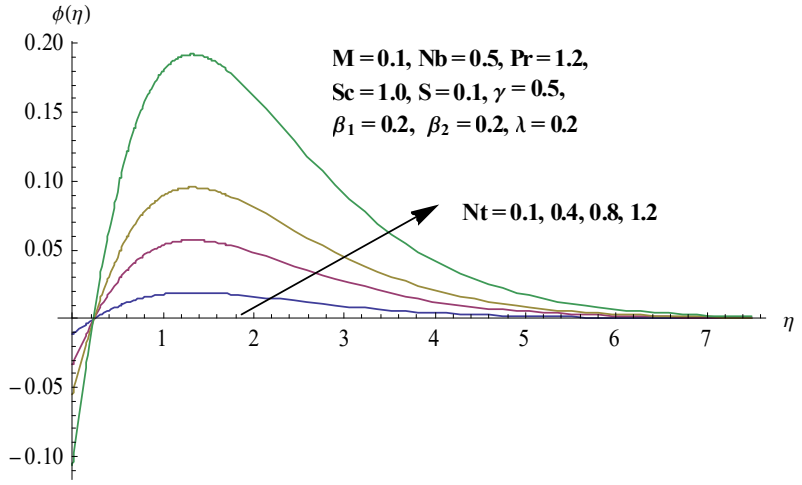

Fig. 3.19: Influence of thermophoresis parameter Nt on concentration profile $\phi(\eta)$.

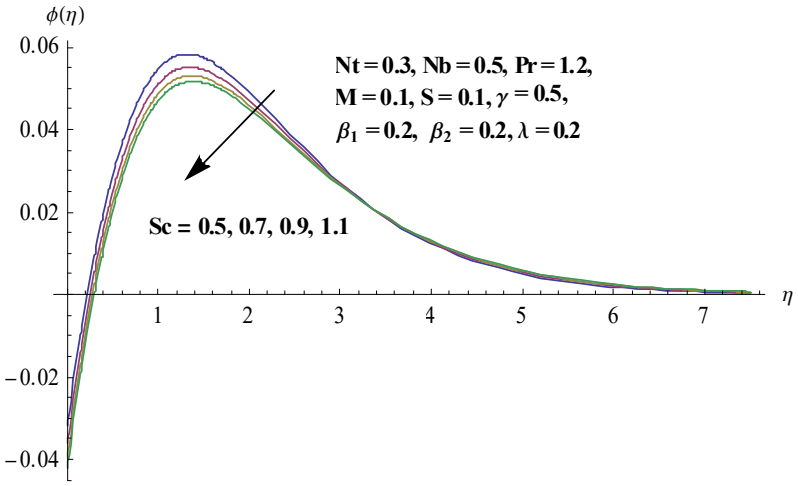

Fig. 3.20: Influence of Schmidt number Sc on concentration profile $\phi(\eta)$.

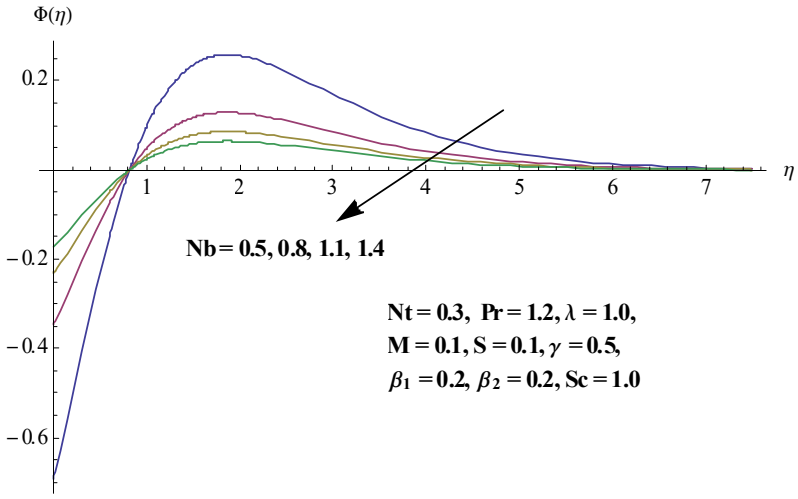

Fig. 3.21: Influence of Brownian motion parameter Nb on concentration profile $\phi(\eta)$.

Table 3.2: Numerical values of local Nusselt number $\left(-\theta'(0)\right)$ for different values of β_1, $\beta_{2,}$ λ, S, γ, Nt, Nb, Sc, Pr and M.

β_1	β_2	λ	S	γ	Nt	Nb	Sc	Pr	$-\theta'(0)$	
									$M = 0.0$	$M = 0.5$
0.0	0.2	0.2	0.1	0.5	0.3	0.5	1.0	1.2	0.2836	0.2780
0.2									0.2790	0.2727
0.4									0.2741	0.2672
0.2	0.0	0.2	0.1	0.5	0.3	0.5	1.0	1.2	0.2722	0.2648
	0.2								0.2789	0.2727
	0.4								0.2836	0.2783
0.2	0.2	0.0	0.1	0.5	0.3	0.5	1.0	1.2	0.2593	0.2512
		0.5							0.2983	0.2940
		1.0							0.3221	0.3167
0.2	0.2	0.2	0.0	0.5	0.3	0.5	1.0	1.2	0.2961	0.2921
			0.1						0.2790	0.2727
			0.2						0.2537	0.2420
0.2	0.2	0.2	0.1	0.2	0.3	0.5	1.0	1.2	0.1523	0.1504
				0.5					0.2790	0.2727
				0.8					0.3514	0.3414
0.2	0.2	0.2	0.1	0.5	0.0	0.5	1.0	1.2	0.2818	0.2758
					0.3				0.2790	0.2727
					0.5				0.2770	0.2705
0.2	0.2	0.2	0.1	0.5	0.3	0.5	1.0	1.2	0.2790	0.2727
						0.7			0.2790	0.2727
						1.0			0.2790	0.2727
0.2	0.2	0.2	0.1	0.5	0.3	0.5	0.5	1.2	0.2801	0.2739
							1.0		0.2790	0.2727
							1.5		0.2782	0.2719
0.2	0.2	0.2	0.1	0.5	0.3	0.5	1.0	0.5	0.1875	0.1787
								1.0	0.2621	0.2547
								1.5	0.2983	0.2933

Chapter 4

Effects of chemical species and nonlinear thermal radiation on 3D Maxwell nanofluid flow with double stratification

4.1 Mathematical analysis

We consider the three-dimensional MHD steady, incompressible Maxwell nanofluid flow with the impact of non-linear thermal radiation past a stretching surface. Flow analysis is performed in the presence of chemical reaction and double stratification. We adopt a cartesian coordinate system in such a way that the $x-$ and $y-$ axes are directed along the stretching surface while the $z-$ axes is normal to it. Consider $u_w(x) = ax$ and $v_w(y) = by$ (where a, b are positive real numbers) are the velocities of the stretching surface towards the $x-$ and $y-$ directions (Fig. 4.1). Here, the stretching sheet velocities and vary linearly at the distance from the origin.

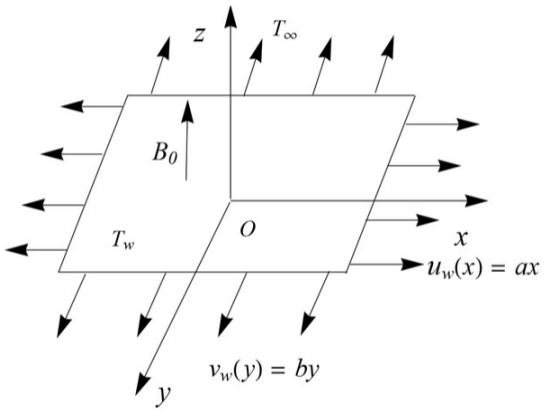

Fig. 4.1 Schematic 3D flow

The resulting boundary layer equations defining the depicted scenario is given as:

$$u_x + v_y + w_z = 0, \tag{4.1}$$

$$uu_x + vu_y + wu_z + \lambda_1 \left(\begin{array}{c} u^2u_{xx} + v^2u_{yy} + w^2u_{zz} + \\ 2uvu_{xy} + 2vwu_{yz} + 2uwu_{xz} \end{array} \right) = \nu u_{zz} - \frac{\sigma B_0^2}{\rho_f}(u + \lambda_1 w u_z), \tag{4.2}$$

$$uv_x + vv_y + wv_z + \lambda_1 \left(\begin{array}{c} u^2v_{xx} + v^2v_{yy} + w^2v_{zz} + \\ 2uvv_{xy} + 2vwv_{yz} + 2uwv_{xz} \end{array} \right) = \nu v_{zz} - \frac{\sigma B_0^2}{\rho_f}(v + \lambda_1 w v_z), \tag{4.3}$$

$$uT_x + vT_y + wT_z = \alpha T_{zz} + \frac{Q}{(\rho c)_f}(T - T_\infty) + \tau \left(D_B (T_z C_z) + \frac{D_T}{T_\infty} (T_z)^2 \right) - \frac{1}{\rho c_p} (q_r)_z, \tag{4.4}$$

$$uC_x + vC_y + wC_z = D_B (C_{zz}) + \frac{D_T}{T_\infty} (T_{zz}) - k_r^2 (C - C_\infty), \tag{4.5}$$

with suitable boundary conditions

$$u = ax, \quad v = by, \quad w = 0,$$

$$T = T_f = T_0 + d_1(x), \; C = C_f = C_0 + d_2(x) \quad \text{at} \quad y = 0,$$

$$T \to T_\infty = T_0 + e_1(x), \; C \to C_\infty = e_2(x) \quad \text{at} \quad y = \infty. \tag{4.6}$$

The radiative heat flux q_r via Rosseland approximation is given by

$$q_r = -\frac{4\sigma^*}{3k^*}\frac{\partial T^4}{\partial z} = -\frac{16\sigma^*}{3k^*}T^3\frac{\partial T}{\partial z}, \tag{4.7}$$

and

$$T = T_\infty[1 + (\theta_w - 1)\theta]. \tag{4.8}$$

Invoking Eq. (4.7) in Eq. (4.4), the temperature equation takes the form

$$uT_x + vT_y + wT_z = \left[\left(\alpha + \frac{1}{\rho c_p}\frac{16\sigma^*}{\partial k^*}T^3\right)T_z\right]_z + \frac{Q}{(\rho c)_f}(T - T_\infty)$$

$$+\tau\left(D_B(T_zC_z) + \frac{D_T}{T_\infty}(T_z)^2\right). \tag{4.9}$$

Dimensionless form of above mathematical model is obtained by using following transformations:

$$\eta = \sqrt{\frac{a}{\nu}}z,\ \theta(\eta) = \frac{T - T_\infty}{T_f - T_0},\ \phi(\eta) = \frac{C - C_\infty}{C_\infty},$$
$$u = axf'(\eta),\ v = ayg'(\eta),\ w = -(av)^{1/2}(f(\eta) + g(\eta)). \tag{4.10}$$

Here, satisfaction of Eq. (3.1) is inevitable. However, Eqs. (3.2) – (3.5) take the form

$$f''' + \left(M^2\beta_1 + 1\right)(f + g)f'' - f'^2 + \beta_1\left(2(f + g)f'f'' - (f + g)^2 f'''\right)$$
$$-M^2 f' = 0, \tag{4.11}$$

$$g''' + \left(M^2\beta_1 + 1\right)(f + g)g'' - g'^2 + \beta_1\left(2(f + g)g'g'' - (f + g)^2 g'''\right)$$
$$-M^2 g' = 0, \tag{4.12}$$

$$\theta'' + (f + g)\Pr\theta' - \Pr\left(f'S_1 + f'\theta\right) + \frac{Nb}{Nt}\Pr\theta'\phi' + \Pr\theta'^2 + \Pr S\theta$$
$$+\frac{4}{3}Rd\left(\begin{array}{c}\left((\theta_w - 1)^3\theta^3\theta''\right) + 3(\theta_w - 1)^2\theta''\theta^2 + \theta'' + 3(\theta_w - 1)^3\theta'^2\theta^2 + \\ 3(\theta_w - 1)\theta''\theta + 3(\theta_w - 1)\theta'^2 + 6(\theta_w - 1)^2\theta'^2\theta\end{array}\right) = 0, \tag{4.13}$$

$$\phi'' + \frac{Nt}{Nb}\theta'' + Sc\,(f+g)\,\phi' - f'\,(S_2+\phi)\,Sc - k\phi = 0. \tag{4.14}$$

$$f = g = 0,\ f' = 1,\ g' = \lambda,\ \theta = (1-S_1),\quad \phi = (1-S_2)\ \text{ as }\ \eta \to 0,$$

$$f' \to 0,\ \ g' \to 0,\ \theta \to 0,\ \ \phi \to 0\ \text{ as } \eta \to \infty. \tag{4.15}$$

The values of above mentioned parameters are

$$\beta_1 = \lambda_1 a,\ M^2 = \frac{\sigma B_0^2}{\rho_f a},\ Nb = \frac{\tau D_B C_\infty}{\nu},\ Nt = \frac{\tau D_T\,(T_f - T_0)}{\nu T_\infty},$$

$$\Pr = \frac{\nu}{\alpha},\ S = \frac{Q}{a\,(\rho c)_f},\ Rd = \frac{4\sigma^* T_\infty^3}{Kk^*},\ Sc = \frac{\nu}{D_B},$$

$$Sc = \frac{\nu}{D_B},\ k = \frac{k_r^2}{a},\ S_1 = \frac{e_1}{d_1},\ S_2 = \frac{e_2}{d_2}. \tag{4.16}$$

The dimensional form of local Nusselt number is given by:

$$Nu_x = \frac{x q_w}{K\,(T_f - T_0)},\quad q_w = -K\,(T_z)_{z=0} + (q_r)_w\,, \tag{4.17}$$

The local Nusselt number in dimensionless form is appended below:

$$Nu_x\,\mathrm{Re}_x^{-1/2} = -[1 + Rd\{1 + (\theta_w - 1)\,\theta\,(0)\}^3]\theta'\,(0)\,. \tag{4.18}$$

.

4.2 Series solutions

Following the homotopy analysis method (HAM), the initial guesses $(f_0, g_0\ , \theta_0,\ \phi_0)$ and linear operators $(\mathcal{L}_f, \mathcal{L}_g,\ \mathcal{L}_\theta,\ \mathcal{L}_\phi)$ are selected and given as follows:

$$f_0\,(\eta) = (1 - \exp\,(-\eta))\,,\ g_0 = \lambda\,(1 - \exp\,(-\eta))\,,\ \theta_0\,(\eta) = (1 - S_1),$$

$$\phi_0\,(\eta) = (1 - S_2), \tag{4.19}$$

$$\mathcal{L}_f = f''' - f', \mathcal{L}_g = g''' - g', \mathcal{L}_\theta = \theta'' - \theta,\ \mathcal{L}_\phi = \phi'' - \phi, \tag{4.20}$$

with

$$\mathcal{L}_f \left[B_1 + B_2 \exp(\eta) + B_3 \exp(-\eta)\right] = 0,$$

$$\mathcal{L}_g \left[B_4 + B_5 \exp(\eta) + B_6 \exp(-\eta)\right] = 0,$$

$$\mathcal{L}_\theta \left[B_7 \exp(\eta) + B_8 \exp(-\eta)\right] = 0,$$

$$\mathcal{L}_\phi \left[B_9 \exp(\eta) + B_{10} \exp(-\eta)\right] = 0, \tag{4.21}$$

where B_j $(j = 1 - 10)$ are the arbitrary constants.

4.3 Convergence analysis

Homotopy analysis technique is used to find the series solutions and is highly dependent on auxiliary parameters $\hbar_f, \hbar_g, \hbar_\theta$ and $\hbar_\phi$. These parameters are essential to control and regulate the convergence region of series solutions. The admissible ranges of the auxiliary parameters $\hbar_f, \hbar_g$, $\hbar_\theta$ and $\hbar_\phi$ are $-1.6 \leq \hbar_f \leq -0.2$, $-1.5 \leq \hbar_g \leq -0.3$, $-1.7 \leq \hbar_\theta \leq -0.8$ and $-1.6 \leq \hbar_\phi \leq -0.1$, when $S = 0.1$, $Nt = 0.1$, $Pr = 1.0$, $Nb = 0.3$, $Rd = 0.2$, $\beta_1 = 0.3$, $M = 0.4$, $Sc = 0.8$, $\theta_w = 0.5$, $\lambda = 0.3$ and $S_1 = S_2 = 0.8$. Table 4.1 gives the convergence of HAM solutions. Here, it is examined that momentum, energy and concentration equations displays the convergence at 20th order of approximations. We can see that values obtained in the table are in total alignment to the curves shown in Fig. 4.2. Its also validate both numerical and graphical results.

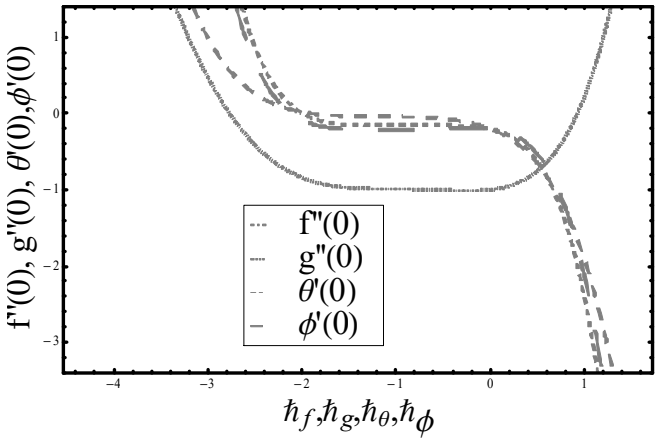

Fig. 4.2 $\hbar-$curves for f, g, θ and ϕ

Table 4.1: Convergence of homotopic solutions for various order of approximations when and $\hbar_f = \hbar_g = -0.9 = \hbar_\theta = \hbar_\phi$.

Order of Approximations	$-f''(0)$	$-g'(0)$	$-\theta'(0)$	$-\phi'(0)$
1	0.99750	0.15980	0.13620	0.18150
5	1.00200	0.15390	0.09212	0.20190
10	0.99880	0.15360	0.07378	0.21070
20	0.99660	0.15400	0.06439	0.21430
25	0.99660	0.15400	0.06439	0.21430

4.4 Results and discussion

The goal of this section is to portray the important characteristics of arising parameters on velocity components, temperature and concentration distributions. Various parameters like the Deborah number in term of relaxation times β_1, magnetic parameter M, Schmidt number Sc, Prandtl number Pr, heat generation/absorption parameter S, Brownian motion parameter Nb, thermophoresis parameter Nt, temperature ratio parameter θ_w, chemical reaction parameter k and radiation parameter Rd are discussed on velocity, temperature and nanoparticles concentration profile. Thermal and concentration parameters S_1 and S_2 on the temperature profile $\theta(\eta)$ and nanoparticles concentration profile $\phi(\eta)$ are also discussed and analyzed. Figure 4.3

shows the impact of Deborah number β_1 on the velocity distribution. It indicates that an increase in Deborah number β_1 causes a decay in velocity profile $f'(\eta)$ and related thickness of thermal layer. When Deborah number enhances consequently more resistance to flow of the fluid is observed. Features of magnetic parameter M on the velocity distribution are depicted in Figure 4.4. It is concluded that the velocity distribution decreases for large M. Its due to the fact that when M is low then heat decreases. As the result temperature difference between magnetic parameter and heat decrease which cause decay in velocity distribution. Figure 4.5 defines the effect of Deborah number β_1 on velocity distribution $g'(\eta)$. Velocity shows decreasing behavior for larger β_1. Since Deborah number is ratio of relaxation to the observation times, so relaxation time increase when Deborah number enhances. Consequently, more resistance to flow of the fluid is provided. Magnetic parameter M on the velocity profile $g'(\eta)$ is shown in figure 4.6. It elucidates that when the values of magnetic parameter are larger then boundary layer thickness becomes lower. Magnetic parameter M links with the Lorentz force. Greater values of magnetic parameter M corresponds to a stronger Lorentz force which causes an increment in related thickness of thermal layer and temperature profile. Here $M = 0$, tends to a hydrodynamic flow situation. Change in velocity profile $g'(\eta)$ for different values of ratio parameter λ is sketched in figure 4.7. Here, velocity and thickness of thermal layer show an increasing behavior for larger values of ratio parameter λ. Figure 4.8 illustrates the variation of Prandtl number Pr on temperature profile $\theta(\eta)$. It is seen that for large values of Prandtl number Pr temperature profile decreases. As Prandtl number is the ratio of momentum to thermal diffusivities. Increment in Prandtl number leads to weaker thermal diffusivity and stronger momentum diffusivity. Here, due to which lower temperature it is noticed that weaker thermal diffusivity is more poweful over the stronger momentum diffusivity. Figure 4.9 is sketched to portray the behavior of thermophoresis parameter Nt on temperature profile $\theta(\eta)$. Both temperature $\theta(\eta)$ and thickness of thermal layer are increased for increasing values of thermophoresis parameter Nt. Greater values of thermophoresis parameter Nt causes an increment in the thermophoresis force which leads to move nanoparticles from hot to cold surfaces and similarly it increases the temperature and thickness of thermal layer. Figure 4.10 depicts that for an increasing values of Brownian motion parameter Nb leads to a greater temperature profile $\theta(\eta)$. The motion of fluid particles rise when Nb enhances. As a result more heat generate which boosts the

temperature. Figure 4.11 shows the behavior against temperature ratio parameter θ_w. Here, $\theta(\eta)$ is an increasing function of θ_w. Figure 4.12 plotted to show the curves of $\theta(\eta)$ for various terms of Rd at other variables are fixed. It can be judge that Rd depicts the temperature and its parallel layer thickness become thicker. Physically, it is clear that in radiation process, heat is generated in the working liquid, which cause to rise in thermal field. Figure 4.13 indicates that variations in temperature profile $\theta(\eta)$ for distinct values of heat generation/absorption parameter. Here, $S > 0$, leads to heat generation and $S < 0$, corresponds to heat absorption. It is surely seen that temperature profile $\theta(\eta)$ and thickness of thermal layer are higher in the case of heat generation as compare to the heat absorption case. Figure 4.14 is drawn to analyze the diferesces in temperature for various values of thermal stratification parameter S_1. Here we noticed that the temperature is a decreasing function of thermal stratification parameter S_1. Figure 4.15 plotted to show that an increase in Schmidt number Sc corresponds to decay in nanoparticles concentration distribution $\phi(\eta)$. There is an inverse relationship between Schmidt number and the Brownian diffusion coefficient. Greater values of Schmidt number Sc leads to a lower Brownian diffusion coefficient, which causes reduction in nanoparticles concentration. Figure 4.16 shows the increasing behavior of thermophoresis parameter Nt in concentration profile $\phi(\eta)$. The decending behavior in concentration distribution $\phi(\eta)$ of Brownian motion parameter Nb is drawn in figure 4.17. In nanofluid flow, due to the existence of nanoparticles, the Brownian motion occurs and with an increment in the Brownian motion parameter Nb the Brownian motion is affected and similarly the boundary layer thickness decreases. Figure 4.18 portrays the concentration field for different values of chemical reaction parameter k. Large values of chemical reaction parameter k corresponds to reduction in nanoparticles concentration distribution. Figure 4.19 shows the significant aspects of concentration or solutal stratification S_2 on $\phi(\eta)$. Because of large disturbance in molecules of fluid, the reduction in solute nanoparticle concentration occurs which cause to decay in concentration profile $\phi(\eta)$. Concentration relates the decaying nature with the intensity of solutal stratification. Influences of Nt and Pr on the local Nusselt number is shown in Figure 4.20. It is disclosed that the local Nusselt number decreases for increasing values of Nt and Pr.

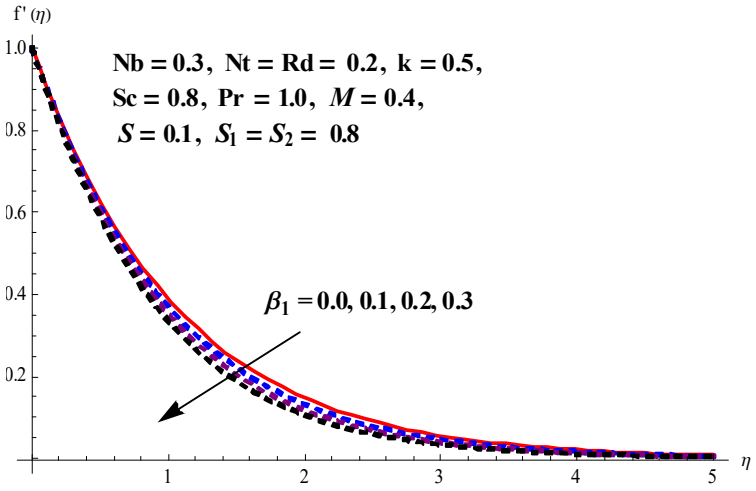

Fig. 4.3: Impact of Deborah number β_1 on $f'(\eta)$.

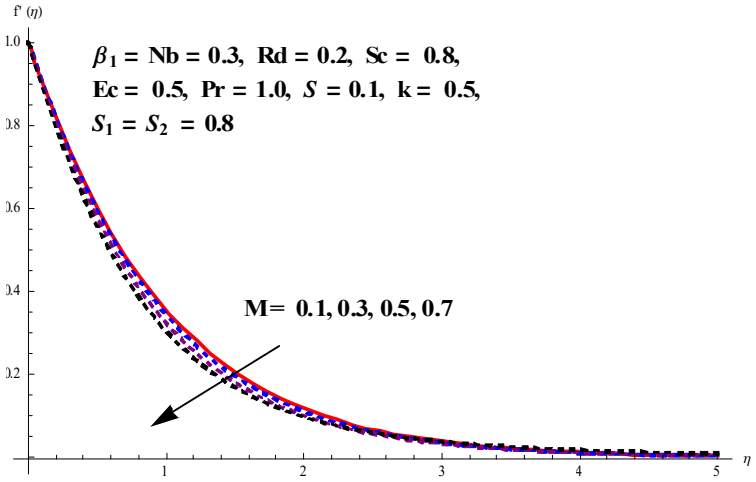

Fig. 4.4: Impact of magnetic parameter M on $f'(\eta)$.

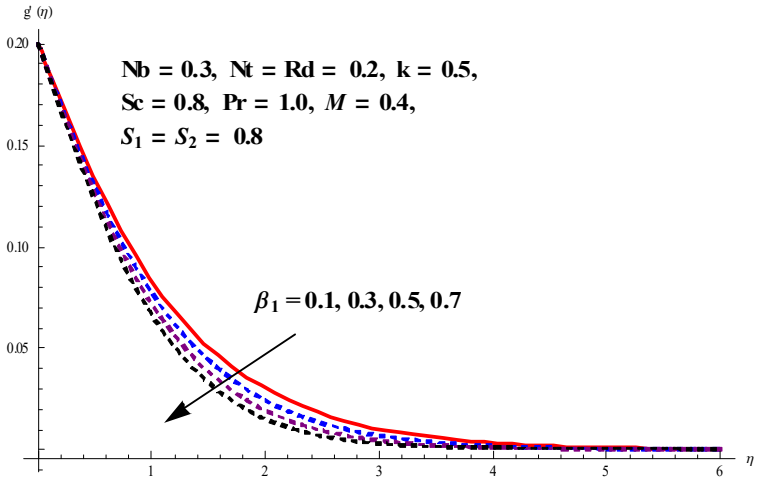

Fig. 4.5: Impact of Deborah number β_1 on $g'(\eta)$.

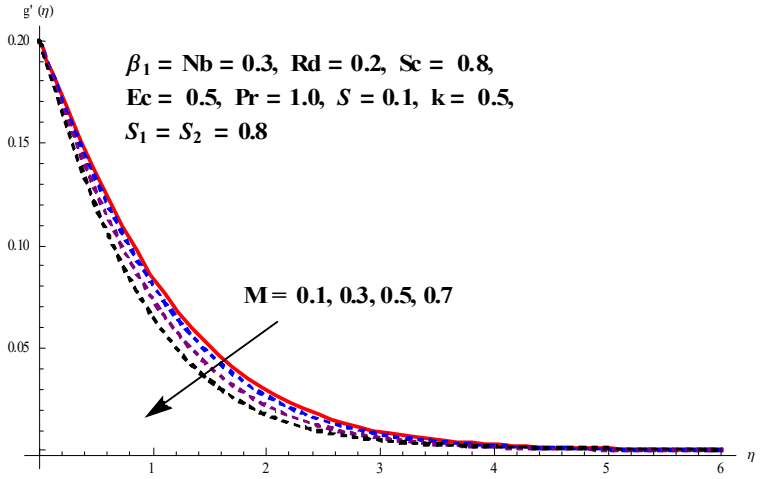

Fig. 4.6: Impact of magnetic parameter M on $g'(\eta)$.

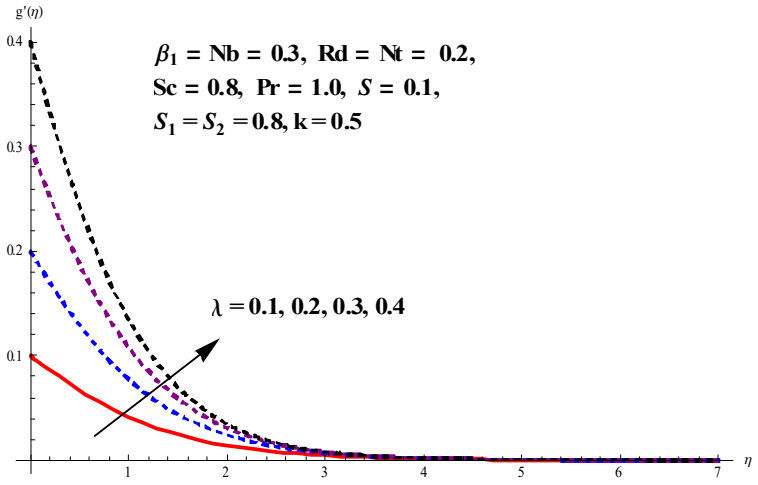

Fig. 4.7: Impact of ratio parameter λ on $g'(\eta)$.

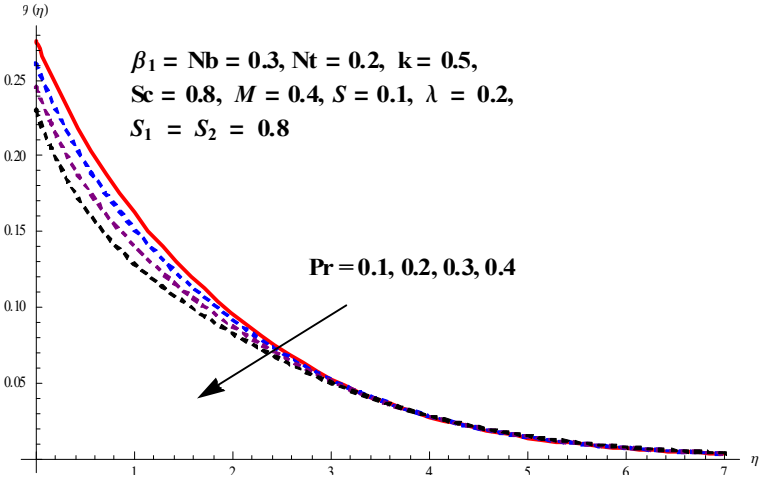

Fig. 4.8: Impact of Prandtl number Pr on $\theta(\eta)$.

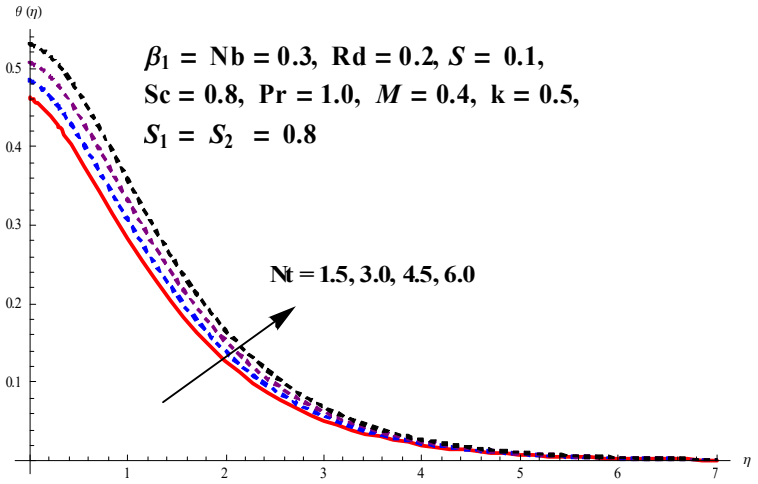

Fig. 4.9: Impact of thermophoresis parameter Nt on $\theta(\eta)$.

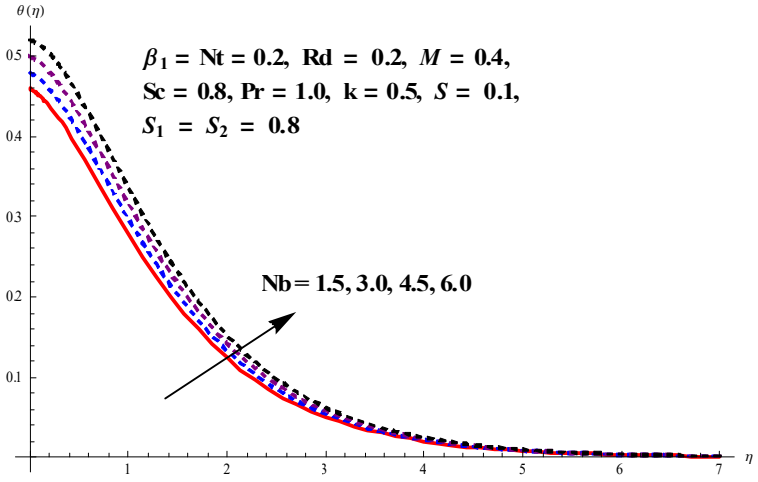

Fig. 4.10: Impact of Brownian motion parameter Nb on $\theta(\eta)$.

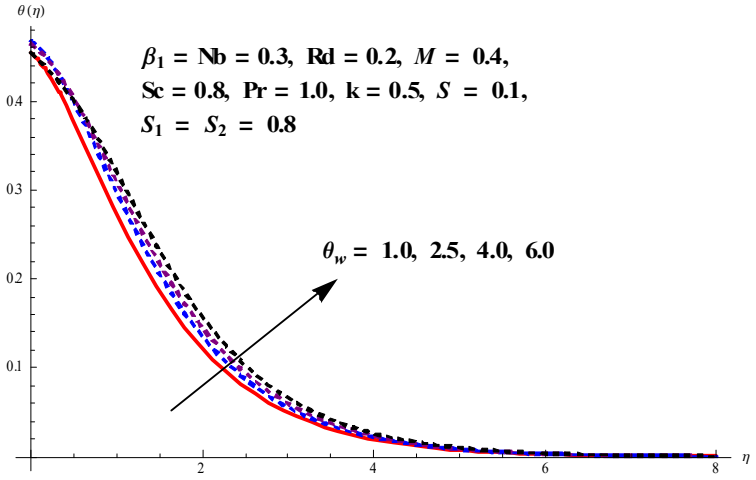

Fig. 4.11: Impact of temperature ratio parameter θ_w on $\theta(\eta)$.

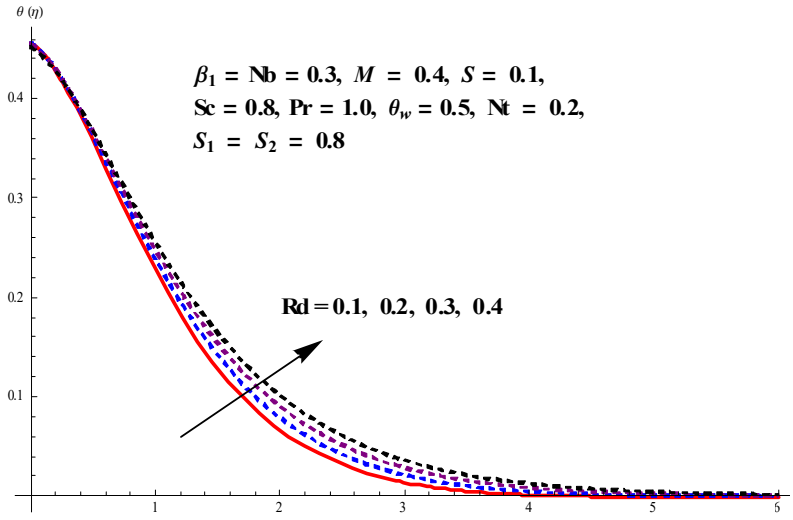

Fig. 4.12: Impact of radiation parameter Rd on $\theta(\eta)$.

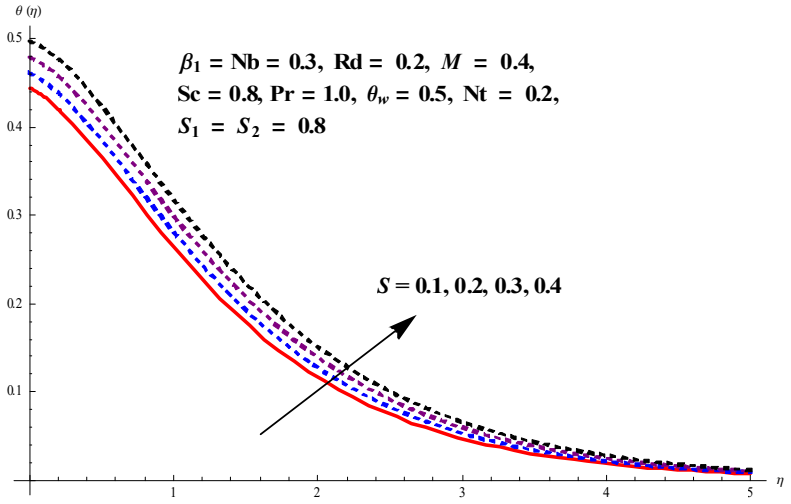

Fig. 4.13: Impact of heat generation parameter S on $\theta(\eta)$.

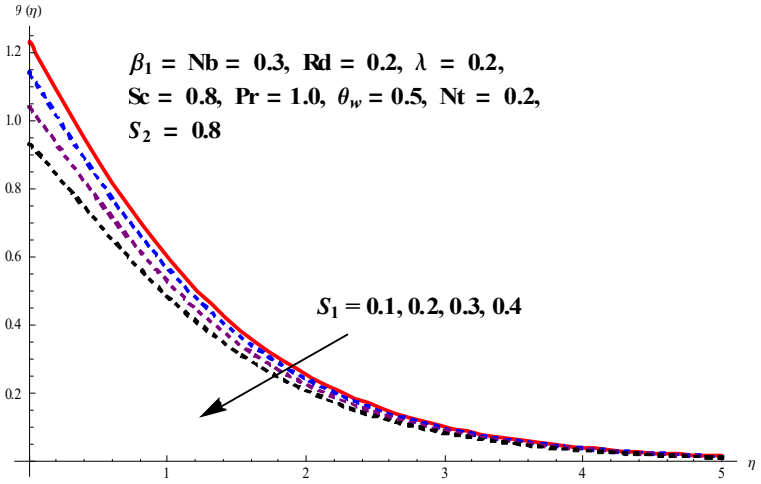

Fig. 4.14: Impact of thermal stratification parameter S_1 on $\theta(\eta)$.

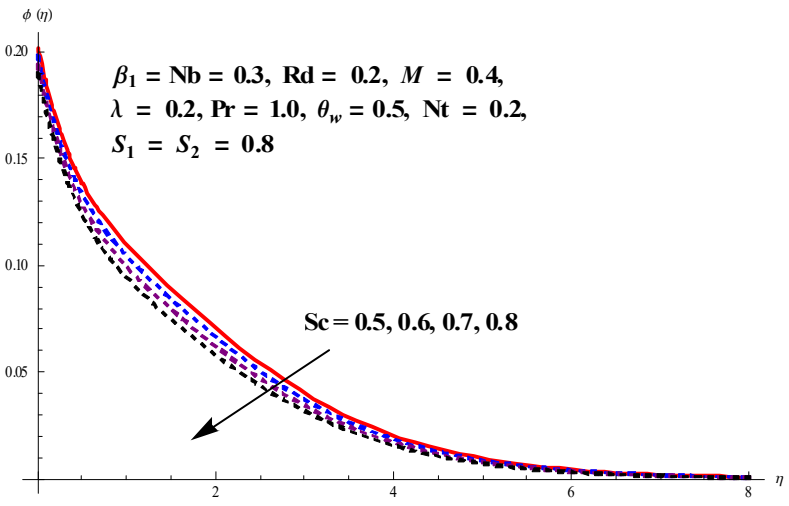

Fig. 4.15: Impact of Schmidt number Sc on $\phi(\eta)$.

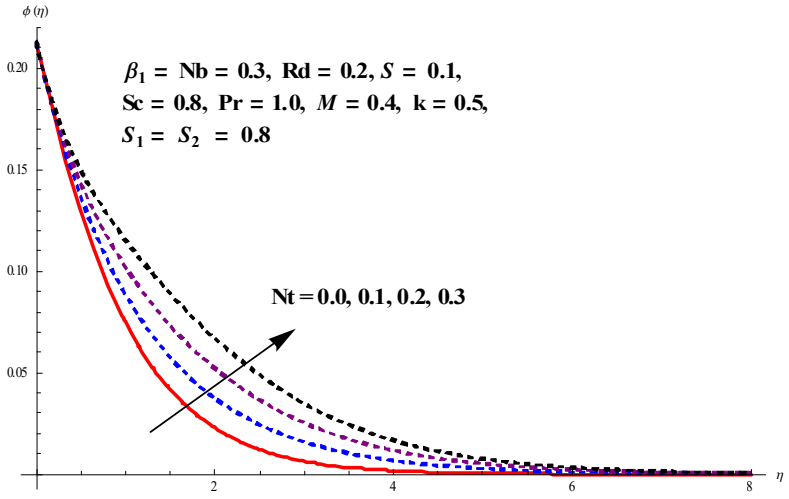

Fig. 4.16: Impact of thermophoresis parameter Nt on $\phi(\eta)$.

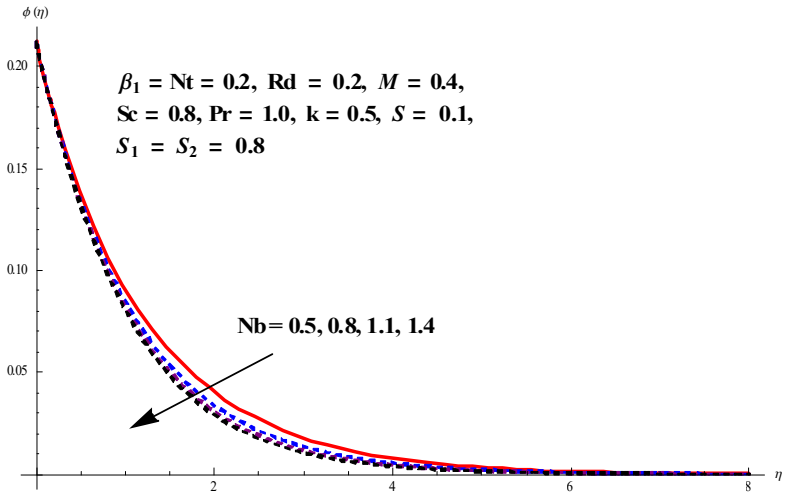

Fig. 4.17: Impact of Brownian motion parameter Nb on $\phi(\eta)$.

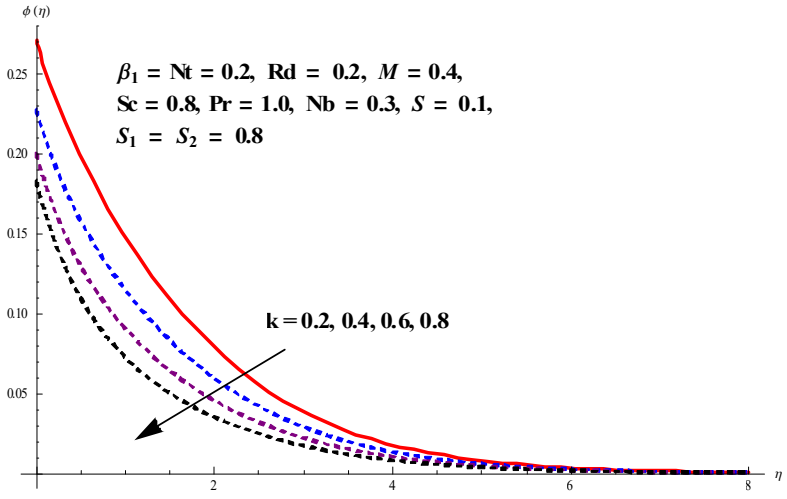

Fig. 4.18: Impact of chemical reaction parameter k on $\phi(\eta)$.

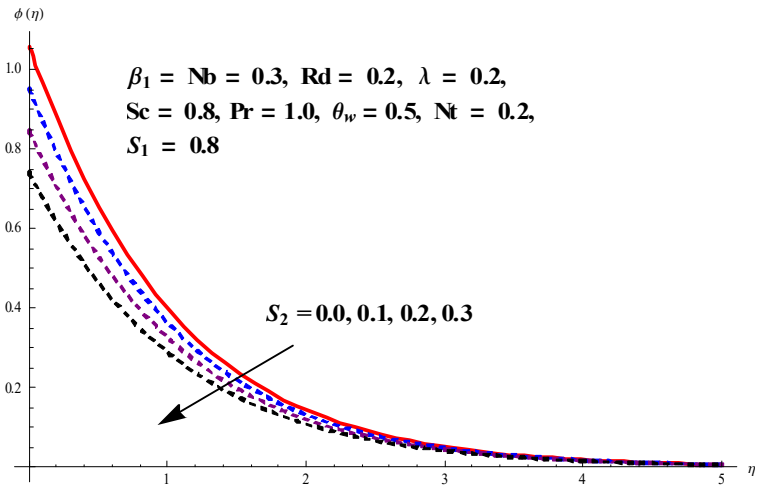

Fig. 4.19: Impact of concentration stratification parameter S_2 on $\phi(\eta)$.

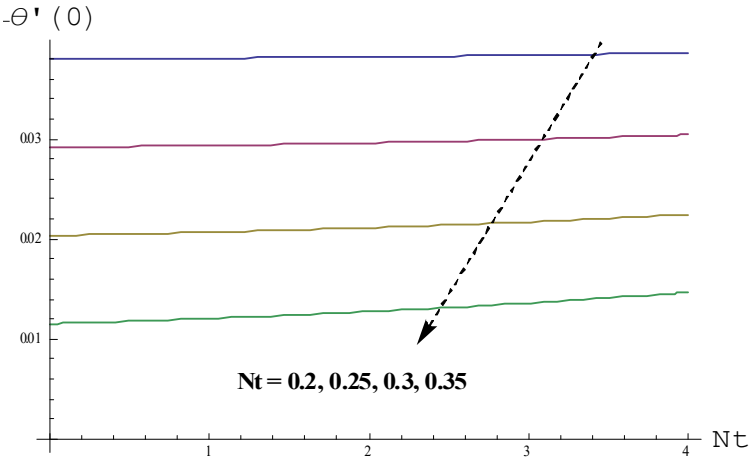

Fig. 4.20: Impact of $Nu_x \operatorname{Re}_x^{-1/2}$ versus Nt and Pr.

Chapter 5

Conclusions and Future work

In this thesis two problems have been analyzed where first problem is about review paper and second problem is the extension work for it. Conclusion of both the problems are as following:

5.1 Chapter 3

Simultaneous effects of magnetic field and convective condition in three-dimensional (3D) flow of an Oldroyd-B nanoliquid is studied in the existence of heat generation/absorption. The main outcomes of this analysis are listed below:

- Temperature and nanoparticles concentration are higher for larger values of Deborah number in terms of relaxation time.
- Impacts of Deborah number in terms of retardation time are qualitatively similar for velocity distributions.
- Temperature and nanoparticles concentration profiles show increasing behavior for larger values of magnetic parameter.
- An increment in ratio parameter leads to lower temperature and nanoparticles concentration profiles.
- Larger values of Biot number cause an increment in temperature and nanoparticles concentration distributions.

5.2 Chapter 4

In the current exploration, we have studied the flow of Maxwell nanofluid flow with impact of non-linear thermal radiation, chemical reaction, thermal and solutal stratification. Analytical solution of the problem is extracted with the help of renowned Homotopy Analysis method. The salient features of the present investigation are appended as follows:

- Impacts of Brownian motion parameter on the concentration and temperature profiles are opposite.
- Enhancing values of Deborah number will lead to increase the velocity distributions.
- Concentration distribution decreases for higher values of chemical reaction parameter k.
- Thermally stratified parameter reduce the temperature field.
- Solutal stratification parameter decrease the concentration profile.
- Local Nusselt number reduces for higher values of Nt and Pr.

5.3 Future work

The present analysis can be extended to the following models as well:

- The fluid flow may be extended to the any other non-Newtonian fluid.
- The momentum equation may be enhanecd by adding the effects of Darcy-Forchheimer and buoyancy effects.
- The energy equation can be enhanced by adding the cattaneo-christov heat flux.
- The impact of Arrhenis activation energy may be added.
- The model may be extended to homogeneous heterogeneous reactions.
- The boundary conditions may be exchanged with melting heat, convective heat and mass transfer.

Bibliography

[1] Ramzan, M., Bilal, M., Chung, J. D., & Farooq, U. (2016). Mixed convective flow of Maxwell nanofluid past a porous vertical stretched surface–An optimal solution. Results in Physics, 6, 1072-1079.

[2] Hussain, T., Hussain, S., & Hayat, T. (2016). Impact of double stratification and magnetic field in mixed convective radiative flow of Maxwell nanofluid. Journal of Molecular Liquids, 220, 870-878.

[3] Bai, Y., Liu, X., Zhang, Y., & Zhang, M. (2016). Stagnation-point heat and mass transfer of MHD Maxwell nanofluids over a stretching surface in the presence of thermophoresis. Journal of Molecular Liquids, 224, 1172-1180.

[4] Ramzan, M., Bilal, M., & Chung, J. D. (2017). Influence of homogeneous-heterogeneous reactions on MHD 3D Maxwell fluid flow with Cattaneo-Christov heat flux and convective boundary condition. Journal of Molecular Liquids, 230, 415-422.

[5] Jusoh, R., Nazar, R., & Pop, I. (2017). Flow and heat transfer of magnetohydrodynamic three-dimensional Maxwell nanofluid over a permeable stretching/shrinking surface with convective boundary conditions. International Journal of Mechanical Sciences, 124, 166-173.

[6] Hayat, T., Qayyum, S., Waqas, M., & Alsaedi, A. (2016). Thermally radiative stagnation point flow of Maxwell nanofluid due to unsteady convectively heated stretched surface. Journal of molecular liquids, 224, 801-810.

[7] Sheikholeslami, M., & Ganji, D. D. (2013). Heat transfer of Cu-water nanofluid flow between parallel plates. Powder Technology, 235, 873-879.

[8] Ellahi, R. (2013). The effects of MHD and temperature dependent viscosity on the flow of non-Newtonian nanofluid in a pipe: analytical solutions. Applied Mathematical Modelling, 37(3), 1451-1467.

[9] Ramzan, M., & Bilal, M. (2016). Three-dimensional flow of an elastico-viscous nanofluid with chemical reaction and magnetic field effects. Journal of Molecular Liquids, 215, 212-220.

[10] Kameswaran, P. K., Shaw, S., Sibanda, P., & Murthy, P. V. S. N. (2013). Homogeneous–heterogeneous reactions in a nanofluid flow due to a porous stretching sheet. International journal of heat and mass transfer, 57(2), 465-472.

[11] Hussain, T., Shehzad, S. A., Hayat, T., Alsaedi, A., Al-Solamy, F., & Ramzan, M. (2014). Radiative hydromagnetic flow of Jeffrey nanofluid by an exponentially stretching sheet. Plos One, 9(8), e103719.

[12] Hussain, T., Shehzad, S. A., Alsaedi, A., Hayat, T., & Ramzan, M. (2015). Flow of Casson nanofluid with viscous dissipation and convective conditions: a mathematical model. Journal of Central South University, 22(3), 1132-1140.

[13] Hayat, T., Hussain, Z., Alsaedi, A., & Mustafa, M. (2017). Nanofluid flow through a porous space with convective conditions and heterogeneous–homogeneous reactions. Journal of the Taiwan Institute of Chemical Engineers, 70, 119-126.

[14] Ramzan, M., Bilal, M., Chung, J. D., & Mann, A. B. (2018). On MHD radiative Jeffery nanofluid flow with convective heat and mass boundary conditions. Neural Computing and Applications, 30(9), 2739-2748.

[15] Mabood, F., Shateyi, S., Rashidi, M. M., Momoniat, E., & Freidoonimehr, N. (2016). MHD stagnation point flow heat and mass transfer of nanofluids in porous medium with radiation, viscous dissipation and chemical reaction. Advanced Powder Technology, 27(2), 742-749.

[16] Ramzan, M., Bilal, M., & Chung, J. D. (2017). Radiative Williamson nanofluid flow over a convectively heated Riga plate with chemical reaction-A numerical approach. Chinese journal of physics, 55(4), 1663-1673.

[17] Ramzan, M., Bilal, M., & Chung, J. D. (2017). Radiative Williamson nanofluid flow over a convectively heated Riga plate with chemical reaction-A numerical approach. Chinese journal of physics, 55(4), 1663-1673.

[18] Ibrahim, W., & Makinde, O. D. (2013). The effect of double stratification on boundary-layer flow and heat transfer of nanofluid over a vertical plate. Computers & Fluids, 86, 433-441.

[19] Hayat, T., Farooq, M., Khan, M. I., Waqas, M., Alsaedi, A., & Khan, M. I. (2016). MHD stagnation point flow of viscoelastic nanofluid with non-linear radiation effects. Journal of molecular liquids, 221, 1097-1103.

[20] Srinivasacharya, D., & Upendar, M. (2013). Effect of double stratification on MHD free convection in a micropolar fluid. Journal of the Egyptian Mathematical Society, 21(3), 370-378.

[21] Hayat, T., Hussain, T., Shehzad, S. A., & Alsaedi, A. (2014). Thermal and concentration stratifications effects in radiative flow of Jeffrey fluid over a stretching sheet. Plos one, 9(10), e107858.

[22] Ramzan, M., Gul, H., & Chung, J. D. (2017). Double stratified radiative Jeffery magneto nanofluid flow along an inclined stretched cylinder with chemical reaction and slip condition. The European Physical Journal Plus, 132(11), 456.

[23] Babu, M. J., & Sandeep, N. (2017). UCM flow across a melting surface in the presence of double stratification and cross-diffusion effects. Journal of Molecular Liquids, 232, 27-35.

[24] Ramzan, M., Bilal, M., & Chung, J. D. (2017). Radiative flow of Powell-Eyring magneto-nanofluid over a stretching cylinder with chemical reaction and double stratification near a stagnation point. PloS one, 12(1), e0170790.

[25] Rehman, K. U., Malik, M. Y., Makinde, O. D., & Malik, A. A. (2017). A comparative study of nanofluids flow yields by an inclined cylindrical surface in a double stratified medium. The European Physical Journal Plus, 132(10), 427.

[26] Ramzan, M., Bilal, M., & Chung, J. D. (2017). Effects of thermal and solutal stratification on Jeffrey magneto-nanofluid along an inclined stretching cylinder with thermal radiation and heat generation/absorption. International Journal of Mechanical Sciences, 131, 317-324.

[27] Daniel, Y. S., Aziz, Z. A., Ismail, Z., & Salah, F. (2017). Double stratification effects on unsteady electrical MHD mixed convection flow of nanofluid with viscous dissipation and Joule heating. Journal of applied research and technology, 15(5), 464-476.

[28] Khan, M. I., Waqas, M., Hayat, T., Khan, M. I., & Alsaedi, A. (2017). Behavior of stratification phenomenon in flow of Maxwell nanomaterial with motile gyrotactic microorganisms in the presence of magnetic field. International Journal of Mechanical Sciences, 131, 426-434.

[29] Hayat, T., Waqas, M., Shehzad, S. A., & Alsaedi, A. (2016). On 2D stratified flow of an Oldroyd-B fluid with chemical reaction: an application of non-Fourier heat flux theory. Journal of Molecular Liquids, 223, 566-571.

[30] Rashad, A. M., Abbasbandy, S., & Chamkha, A. J. (2014). Mixed convection flow of a micropolar fluid over a continuously moving vertical surface immersed in a thermally and solutally stratified medium with chemical reaction. Journal of the Taiwan Institute of Chemical Engineers, 45(5), 2163-2169.

[31] Zeeshan, A., Shehzad, N., & Ellahi, R. (2018). Analysis of activation energy in Couette-Poiseuille flow of nanofluid in the presence of chemical reaction and convective boundary conditions. Results in physics, 8, 502-512.

[32] Animasaun IL. Dynamics of unsteady MHD convective flow with thermophoresis of particles and variable thermo-physical properties past a vertical surface moving through binary mixture. Open J Fluid Dyn 2015;5:106e20.

[33] Animasaun IL. Effects of thermophoresis, variable viscosity and thermal conductivity on free convective heat and mass transfer of non-darcian MHD dissipative Casson fluid flow with suction and nth order of chemical reaction.

[34] Animasaun IL. 47nm aluminawaternanofluid flow within boundary layer formed on upper horizontal surface of paraboloid of revolution in the presence of quarticautocatalysischemical reaction. Alexandria Eng J 2016.

[35] Nagendramma, V., Leelarathnam, A., Raju, C. S. K., Shehzad, S. A., & Hussain, T. (2018). Doubly stratified MHD tangent hyperbolic nanofluid flow due to permeable stretched cylinder. Results in Physics, 9, 23-32.

[36] Waqas, M., Hayat, T., Shehzad, S. A., & Alsaedi, A. (2018). Transport of magnetohydrodynamic nanomaterial in a stratified medium considering gyrotactic microorganisms. Physica B: Condensed Matter, 529, 33-40.

[37] Abbasi, F. M., Shehzad, S. A., Hayat, T., & Alhuthali, M. S. (2016). Mixed convection flow of jeffrey nanofluid with thermal radiation and double stratification. Journal of Hydrodynamics, Ser. B, 28(5), 840-849.

[38] Paul, A., & Deka, R. K. (2017). Unsteady natural convection flow past an infinite cylinder with thermal and mass stratification. International Journal of Engineering Mathematics, 2017.

[39] Rehman, K. U., Khan, A. A., Malik, M. Y., & Pradhan, R. K. (2017). Combined effects of Joule heating and chemical reaction on non-Newtonian fluid in double stratified medium: A numerical study. Results in physics, 7, 3487-3496.

[40] Mishra, S. R., Pattnaik, P. K., & Dash, G. C. (2015). Effect of heat source and double stratification on MHD free convection in a micropolar fluid. Alexandria Engineering Journal, 54(3), 681-689.